

Isomer-sensitive characterization of low temperature oxidation reaction products by coupling a jet-stirred reactor to an electron/ion coincidence spectrometer: case of *n*-pentane

Jérémy Bourgalais¹, Zied Goud², Olivier Herbinet³, Gustavo A. Garcia⁴, Philippe Arnoux²,
Zhandong Wang⁵, Luc-Sy Tran⁶, Guillaume Vanhove⁶, Majdi Hochlaf², Laurent Nahon⁴,
Frédérique Battin-Leclerc³

¹LATMOS/IPSL, UVSQ Université Paris-Saclay, Sorbonne Université, CNRS, Guyancourt, France

²Université Paris-Est, Laboratoire Modélisation et Simulation Multi Echelle, MSME UMR 8208 CNRS, 5 bd Descartes, 77454 Marne-la-Vallée, France.

³Université de Lorraine, Laboratoire Réactions et Génie des Procédés, UPR 3349, Nancy F-54000, France

⁴Synchrotron SOLEIL, L'Orme des Merisiers, Saint-Aubin-BP 48, 91192 Gif-sur-Yvette Cedex, France

⁵National Synchrotron Radiation Laboratory, University of Science and Technology of China, Hefei, Anhui 230029, People's Republic of China

⁶Physicochimie des Processus de Combustion et de l'Atmosphère (PC2A), UMR 8522 CNRS, Université de Lille, F-59000 Lille, France

Physical Chemistry Chemical Physics

*Corresponding author: Frédérique Battin-Leclerc

e-mail: Frederique.battin-leclerc@univ-lorraine.fr

ORCID: 0000-0001-8265-7492

Phone: +33 (0)3 72 74 38 19

Abstract

Through the use of tunable vacuum ultraviolet light generated by the DESIRS VUV synchrotron beamline, a jet-stirred reactor was coupled for the first time to an advanced photoionization mass spectrometer based upon a double imaging PhotoElectron PhotoIon COincidence (i^2 PEPICO) scheme. This new coupling was used to investigate the low-temperature oxidation of *n*-pentane, a prototype molecule for gasoline or Diesel fuels. Experiments were performed under quasi-atmospheric pressure (1.1 bar) with a residence time of 3 s for two equivalence ratios (1/3 and 0.5) with a fuel initial mole fraction of 0.01. The measured time-of-flight mass spectra are in good agreement with those previously obtained with other photoionization mass spectrometers and, like those previous ones, display several m/z peaks for which the related species assignation is ambiguous. This paper shows how the analysis of the coincident mass-tagged Threshold PhotoElectron Spectra (TPES) together with first principle computations, consisting of the determination of the adiabatic ionization energies and the spectra of some products, may assist products identification. The results mostly confirm those previously obtained by photoionization mass spectrometry and gas chromatography, but also allow a more accurate estimation of the 1-pentene/2-pentene mole fraction ratio. Our data also indicate a higher formation of acetone and methyl ethyl ketone than what is predicted by current models, as well as the presence of products that were not previously taken into account, such as methoxyacetylene, methyl vinyl ketone or furanone. The formation of three, four and five membered ring cyclic ethers is confirmed along with linear ketones: 2- and 3-pentanone. A significant general trend in indicating higher amounts of ketones than gas chromatography is noted. Finally, TPES of alkenylhydroperoxides are also provided for the first time and constraints on the isomers identification are provided.

1. Introduction

In a critical energy and environment context, urgent actions need to be undertaken to reduce the emissions of harmful pollutants and to improve the energy efficiency of combustion processes. However, both require a comprehensive understanding of the combustion physico-chemical mechanisms explaining the reactivity behavior as a function of the temperature regime and of the fuel's molecular structure.[1] Detailed kinetic models based on elementary reactions help to address the influence of fuel-replacement and additives on the combustion reactions identifying

chemical pathways that form hazardous pollutants. However, despite a long period of research on conventional petroleum-based fuels and more recently on alternative fuels, understanding detailed combustion processes is still a large and vivid field of investigation. *In situ* diagnostics for real combustion gas-phase environments (*e.g.*, motor engines, gas turbines) are challenging due to the extreme physical parameters (pressure and temperature) and the rich chemistry leading to a wide range of products (hundreds of species involved in thousands of reactions).[2] Thus, fundamental investigations of combustion reactions are carried out in dedicated laboratory environments (*e.g.*, jet-stirred or tubular reactors, laminar premixed low-pressure flames, shock tubes, rapid compression machines)[3–9] under controlled conditions akin to practical systems. Then, reaction mechanisms are built from this fundamental knowledge obtained over a large range of conditions [10,11] and transferred to actual applied combustion processes.[12]

Most of the time laboratory diagnostics rely on Gas Chromatography (GC) often coupled with Mass Spectrometry (MS) to provide an efficient structure-based identification of many stable species for gas-phase chemistry analysis.[13,14] However, GC time resolution does not allow the detection of elusive intermediates present in trace amounts with short lifetimes, in mixtures containing up to several dozens of compounds. Short-lived reaction intermediates play key roles in various gas-phase environments, determining reaction rates and the branching ratios between different product channels, whose identification and quantification are mandatory to improve our understanding of the relevant chemical processes.[15,16] Laser-based non-invasive methods are sensitive and selective diagnostics allowing to detect and quantify reactive intermediates such as free radicals.[17–20] However, most promising techniques are based on Photoionization Mass Spectrometry (PIMS), through the use of synchrotron-generated tunable Vacuum UltraViolet (VUV) light, providing a diagnostic to perform sensitive, multiplex *in situ* chemical analysis for laboratory combustion environments.[5,6,16,21–23] However, synchrotron VUV Photoionization Mass Spectrometry (SVUV-PIMS) allows only in few favorable cases isomer separation and measurement of product branching ratios, including reactive intermediates through the measurement of the photoion intensities as a function of photon energy to obtain the so-called Photoionization Efficiency (PIE) curve of each molecule. [6,16,24–26]

Despite the efficiency of SVUV-PIMS, much more detail on the electronic and molecular structures of the compounds can be obtained from photoelectron spectroscopy measuring the kinetic energy (KE) of the electron ejected upon photoionization.[27,28] For a given species, the

photoelectron intensity is monitored as a function of electron binding energy yielding its PhotoElectron Spectrum (PES), which by integration leads to the PIE curve. Note that the opposite, differentiating the PIE to obtain the PES, is in practice not possible due to the experimental noise amplification. PES offer a better sensitivity and selectivity as each electronic/vibronic state of the ion appears as a distinct peak rather than changes of the slope in PIE spectra. However, PES analysis in a complex environment, such as in combustion studies, results in the sum of all the individual photoelectron spectra, making quantitative analysis difficult. PhotoElectron PhotoIon COincidence (PEPICO) technique extracts both electrons and ions from the ionization events and correlates them, in order to make use of the additional and complementary information from coincident mass spectrometry and photoelectron spectroscopy.[29–34] In the context of combustion processes, PES on mass-selected compounds is extremely useful as it adds to the mass analysis provided by the PIMS method a full electronic/vibrational fingerprint, specific of a given isomer, much richer than the single ionization energy information. Franck-Condon analysis can also provide the ro-vibronic temperature of a given compound. This analytical method has been only recently applied to combustion studies such as flames but its application is fast spreading and has already succeeded in detecting reactive intermediates and final products.[35–41]

In this work we performed for the first time a PEPICO spectroscopy analysis during the oxidation in a Jet-Stirred Reactor (JSR) of *n*-pentane, the simplest alkane presenting a low-temperature reactivity really representative of that of heavier fuels present in gasolines and Diesel fuels. For this reason, the oxidation of this C₅ saturated hydrocarbon has been thoroughly experimentally investigated with reliable detailed kinetic modeling.[42–44] It is therefore a very suitable example to address the capability of the PEPICO technique as an efficient probe for complex combustion environments. The assignment of the experimental spectra is carried out using either PES available in the literature or theoretical spectra as generated using first principle approaches. It should be noted that the ionic products were considered in their electronic ground states, i.e. we omitted the population of their electronic excited states.

2. Methods

2.1 Experimental procedure

Experiments were carried out at the undulator-based DESIRS VUV beamline [45] of synchrotron SOLEIL using the SAPHIRS end-station [46], equipped with the double-imaging photoelectron/photoion (i^2 PEPICO) spectrometer DELICIOUS III [33], to which the JSR oxidation system was adapted. The SAPHIRS experimental setup was already described in the past and only the specificities related to this work are therefore presented here. **Figure 1** displays a scheme of the experimental setup adapted from Krüger et al. [36]

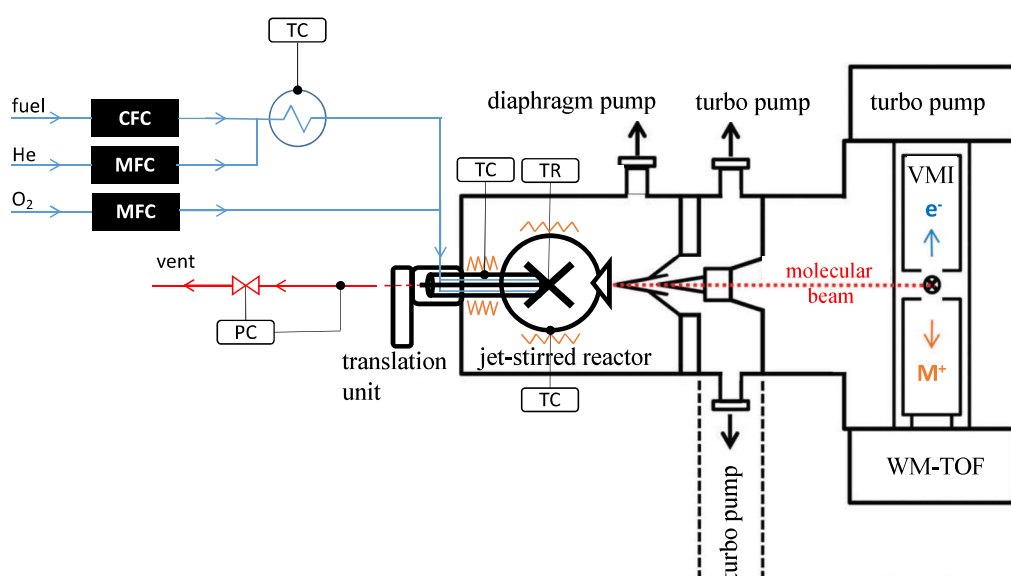


Figure 1. Schematic setup coupling the JSR to the SAPHIRS end-station. The synchrotron radiation is perpendicular to the plane of the figure. CFC is the CoriFlow Controller, MFC are the Mass Flow Controllers, TR is a Temperature Reading, TC are Temperature Controllers and finally PC is a Pressure Controller.

The JSR set-up consists in a quartz sphere (volume $\approx 60 \text{ cm}^3$) connected to annular quartz tubes (an outer tube inside an inner tube) mounted into a CF flange carrying all the diluted reactant gas mixture, which was itself mounted into a 3-axes manipulator. After flowing in the outer tube, the reactant enters the sphere through an injection cross located at the JSR center providing four turbulent jets ensuring the mixing of the gas phase. Contrary to our usual JSR experiments [47], the main gas flow leaves the reactor via a small hole in the injection cross, which is connected to the inner tube. The JSR and the outer tube were heated with Thermocoax wires and temperatures

were varied from 580 to 675 K. The annular preheating zone is used to progressively increase the gas temperature up to the reactor temperature before entering the JSR (the residence time in this annular zone is only a few percent of that in the JSR). The preheating is important to avoid the non-homogeneity of the temperature in the gas phase [48]. Temperature measurements at different positions into the gas phase show that the temperature difference is smaller than 5K. The temperature was controlled using K-type thermocouples. An additional K-type thermocouple, located in the inner tube and only in contact with the burnt gases, was used to monitor the reaction temperature inside the reactor. Experiments were performed at constant temperature and pressure under steady state conditions and under quasi-atmospheric pressure (1.1 bar) with a residence time of 3 s for two equivalence ratios (1/3 and 0.5) with a fuel initial mole fraction of 0.01 and a dilution with He as a buffer gas. Calibrated mass and Coriolis flow controllers were used to control gas and liquid flow rates and the liquid fuel was mixed homogeneously into the gas flow using He as a carrier gas through a controlled evaporation mixing system (CEM, Bronkhorst). The fuel was provided by Sigma-Aldrich (anhydrous, purity $\geq 99\%$), the carrier gas and oxygen by Air Liquide (purities of 99.99% and 99.999%, respectively). Typical JSR conditions established from mixtures of fuel, oxygen and diluent He are summarized in **Table 1**.

C ₅ H ₁₂ (nmlm)	O ₂ (nmlm)	He (nmlm)	total flow (nmlm)	He dilution
6.1	145.9	456.0	607.9	75 mol% of He

Table 1. Typical JSR conditions for a $\phi = 1/3$ pentane-oxygen mixture at 1.1 bar, a residence time of 3 s, and a reaction temperature of 585 K; all flow rates are expressed in nmlm (normal milliliter per minute at 273.15 K and 1 bar).

The gas sample inside the reactor was probed through a quartz nozzle with a 100 μm hole and expanded into a differential pumping chamber (10^{-4} mbar), freezing the composition of the reactor. Then, the molecular beam traversed two consecutive copper skimmers of 1 and 2 mm diameter, expanding further (10^{-6} mbar) towards the ionization chamber where it intersects the ionizing focused VUV beam of DESIRS. Prior to entering the ionization chamber, the light supplied by DESIRS passed through a monochromator, equipped for this experiment with a 200 grooves/mm grating, leading to a flux of ca. 10^{13} ph/s with a spectral resolution of ca. 20 meV at

10 eV. A gas filter located upstream the monochromator and filled with Kr effectively removed high harmonics from the undulator ensuring a spectral purity across the 8-12 eV range used during the experiments.[49] The photon flux was recorded as a function of the photon energy with a dedicated photodiode (AXUV from Optodiode) and used to correct the spectra. The absolute energy scale was calibrated against the 5s and 5s' Kr absorption lines seen in the experimental total ion yields, leading to an absolute accuracy in the energy scale of the order of 4 meV.[50]

The molecular beam crossed the VUV synchrotron radiation at the center of the i²PEPICO spectrometer DELICIOUS III [33]. The coincident electrons and ions resulting from the ionization process are accelerated in opposite directions, analyzed respectively by a Velocity Map Imaging (VMI) spectrometer and a modified Wiley-McLaren time-of-flight imaging spectrometer, and detected in a multi-start/multi-stop coincidence scheme. The coincidence scheme allows the photoelectron images to be tagged by the ion mass and velocity vector. In this work, apart from the mass tagging, only photoelectrons correlated to ions having a net velocity along the molecular beam axis are considered. This removes the background associated to the thermalized gas inside the ionization chamber, and also improves KE and mass resolutions. The resulting mass-filtered ion imaging-filtered photoelectron images are further treated to yield the photoelectron spectra by Abel inversion.[51] The Threshold PES (TPES) are obtained according to the method outlined by Pouilly et al. [52] and Briant et al. [53] where at each photon energy, only electrons along the constant ionic state lines up to a certain eKE_{max} value are counted. Here, a value of $eKE_{\text{max}}=100$ meV has been used, which leads to an electron resolution of around 20 meV, comparable to the photon energy resolution. The total energy resolution of the TPES is then ~ 30 meV. The TPES shows the resonant transitions from the neutral ground state towards vibronic states of the cation, and act as the vibronic fingerprint of the ionic species.[40]

In the following paragraphs, the experimental PE spectra have been used to identify important combustion intermediates including isomers. Literature and calculated reference PE spectra for each mass channel were summed and weighted with appropriate factors to fit the measured PES in the appropriate photon energy range. The fit of the signal for a given mass channel results in an isomeric branching ratio. Relative mole fractions of each isomer could then be estimated by weighting the branching ratios using their respective absolute photoionization cross sections from the literature when available. Note that this estimated relative mole fraction derivation from published absolute photoionization cross sections relies on the assumption that we

can neglect autoionization processes and that the Franck-Condon approximation holds, so that we can consider the TPES overall shape being representative of a fixed-photon energy PES.

2.2 Theoretical PES calculations

Species detected below m/z 70 in this work have been identified using their photoelectron spectra and/or adiabatic Ionization Energies (IEs) found in the literature when available. In the course of a previous study [22] of the low temperature combustion of *n*-pentane the adiabatic ionization energies for several products common to this work have already been calculated using Gaussian at CBS-QB3 level of theory including zero-point energy corrections [54]. This method was assumed to be accurate to better than 50 meV when computing IEs. In the present work, we aim not only at improving the accuracy, but also at providing full simulated photoelectron spectrum for better selectivity when comparing with experimental results.

For $m/z > 70$, state-of-the-art *ab initio* methodology has been used to characterize specific isomers, that lie close in energy making the experimental characterization challenging, for each mass channel detected in the molecular beam. This combination between VUV synchrotron based experiments and high level theoretical calculation has already been used for the study of the electronic structure of nucleobases, including for instance the determination of the structures and the energetics of gas phase cytosine tautomers [55], which are found in biological entities such as DNA and RNA.

The electronic computations consisted on the determination of the equilibrium structures of neutral and ionic species using the PBE0 density functional [56] as implemented in GAUSSIAN09 [57], where the atoms are described using the augmented correlation-consistent aug-cc-pVDZ basis set.[58,59] These full geometry optimizations were done in C_1 point group. The minimal nature of these stationary points is checked after harmonic frequency computations (all frequencies are positive). Zero point vibrational energies (ZPVE) were determined at the anharmonic level as implemented in GAUSSIAN. Afterwards, we generated the PES using the approach implemented in GAUSSIAN 09. Briefly, we performed Franck Condon (FC) analysis and simulated the vibrationally resolved electronic spectra by means of the Time-Independent Adiabatic Hessian Franck-Condon (TI-AH|FC) model.[60–63] The stick spectrum has been convolved with a 20 meV bandwidth Gaussian profile.

For the determination of the IEs, the geometry optimizations are followed by single point computations on the optimized structures using the explicitly correlated coupled cluster with single, double and perturbative triple excitations ((R)CCSD(T)-F12) [64–67] together with the aug-cc-pVTZ basis set in conjunction with the corresponding resolutions of the identity and density fitting functions [68] as generated by MOLPRO.[69] Previous benchmarking by comparison to experimental results showed that the composite scheme PBE0/aug-cc-pVDZ(opt)//(R)CCSD(T)-F12/aug-cc-pVTZ(SP) allows accurate derivation of ionization energies of medium-sized molecular systems (to within ± 0.01 eV).[55,70–74]

Afterwards, the computed spectra were shifted in energy so that the first peak fits with adiabatic ionization energy as computed at the PBE0/aug-cc-pVDZ(opt)//(R)CCSD(T)-F12/aug-cc-pVTZ(SP) level. All the simulated vibrationally resolved electronic spectra in this work are given in the Supplementary Material.

3. Results

Figure 2 shows typical Time-Of-Flight Mass Spectra (TOF-MS) obtained during the oxidation of *n*-pentane at a reactor temperature of 585 K. To show the full range of obtained spectrometric data, **Figure 2a** plots the TOF-MS as a function of *m/z* and photon energy at an equivalence ratio (ϕ) of 0.5. **Figure 2b** shows the related TOF-MS recorded at a 10.5 eV fixed photon energy for two different fuels, $\phi = 1/3$ and 0.5.

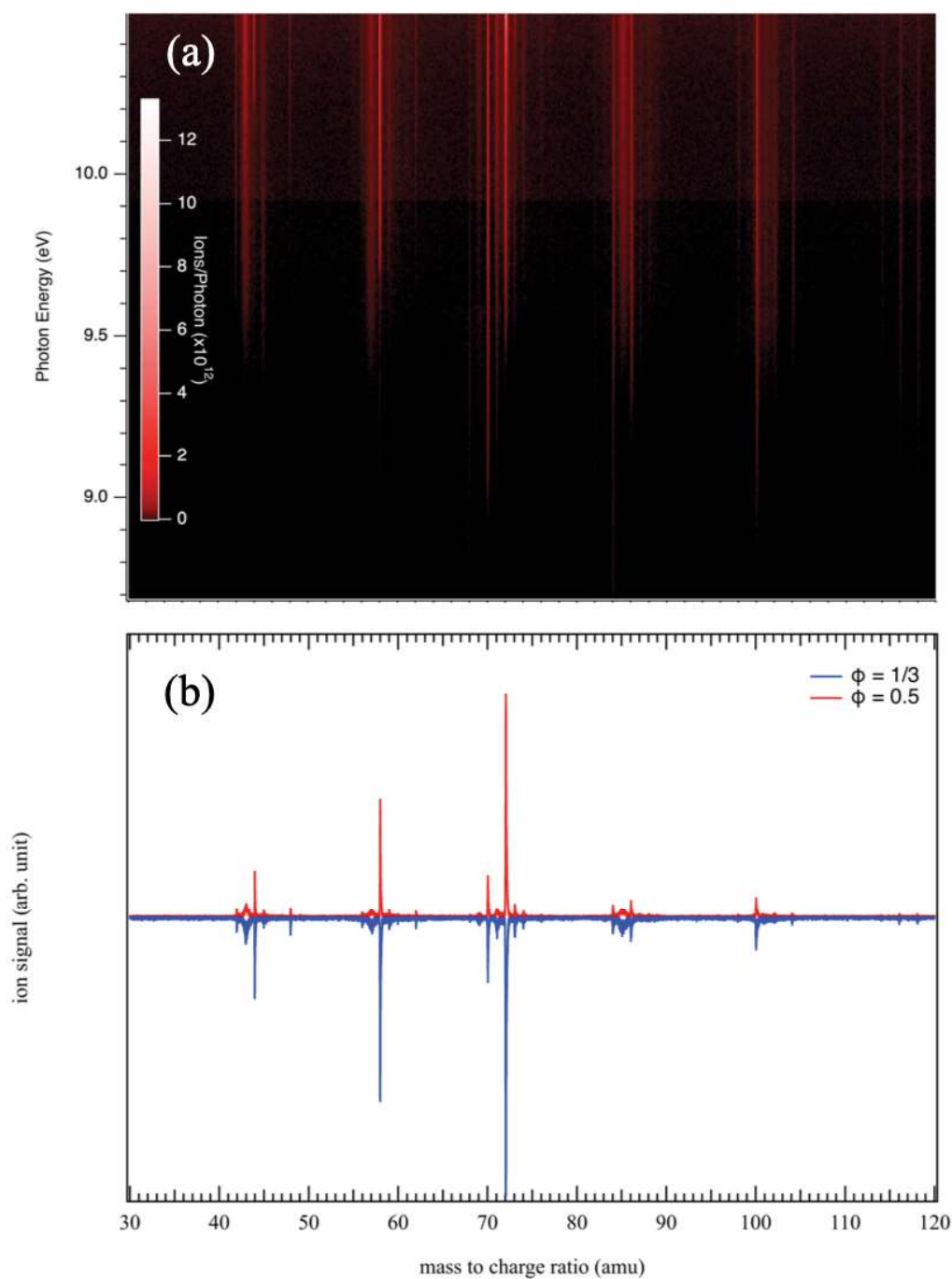


Figure 2. Typical ion signal (a) as a function of m/z and of photon energy (a $\gamma=3$ non-linear colormap, where $\text{intensity}=\text{counts}^{(1/\gamma)}$, has been applied to enhance contrast), and (b) at a fixed energy of 10.5 eV for the $\phi = 1/3$ (blue) and $\phi = 0.5$ (red) conditions during the low temperature combustion of *n*-pentane ($T = 585$ K).

In the following text, two types of experimental data are presented: (i) at a fixed photon energy and (ii) in the scanning mode where the photon energy is scanned in 7 meV steps and the mass-selected photoelectron spectra and mass spectra are recorded as a function of photon energy. The comparison of both $\phi = 1/3$ and $\phi = 0.5$ conditions shows nearly identical TOF-MS and only small variations on the relative intensities of the TOF peaks are observed. The analysis of this work is focused on relatively heavy molecules (> 40 amu) for which experimental or calculated reference PES have been used to identify important combustion intermediates.

Literature presents a couple of experiments [42,44] about *n*-pentane oxidation carried out in JSR under conditions close to those used in this work:

- Fuel inlet mole fraction 0.01
- Equivalence ratios of 0.5, 1 and 2
- Temperatures: 500-1100 K
- Residence time: 2 s
- Pressure: 106.7 kPa
- Four diagnostics (GC with MS for identification and flame ionization detection for quantification, SVUV-PIMS, Single Photoionisation-TOF-MS (SPI-MS), Cavity Ring Down Spectroscopy (cw-CRDS))

Using these different techniques, many species were quantified in these two studies such as acetaldehyde ethylene, propene and cyclic ethers by GC, formaldehyde and H_2O_2 by cw-CDRS, C_1 - C_4 hydroperoxides by SVUV-PIMS and SPI-MS, ketene by SPI-MS. The quantification in SVUV-PIMS and SPIMS analyses was performed using an approximate absolute ionization cross section, estimated by group additivity as proposed by Bobeldijk et al. [75], as there is no data available in the literature for each species and isomers could not be separated for several mass channels. In the following, the simulated mole fractions and production mechanisms are obtained, in the above-described conditions ($\phi = 0.5$), using the model of Bugler et al. [44], which can very well reproduce the JSR results of both studies.

As shown in the comparison displayed in **Figure 3**, the typical mass spectra obtained in this work are consistent with previous studies from the literature about *n*-pentane oxidation at low temperature obtained by SPI-MS [42]: all the m/z species measured by SPI-MS between 50 and 90 are also in our TOF-MS.

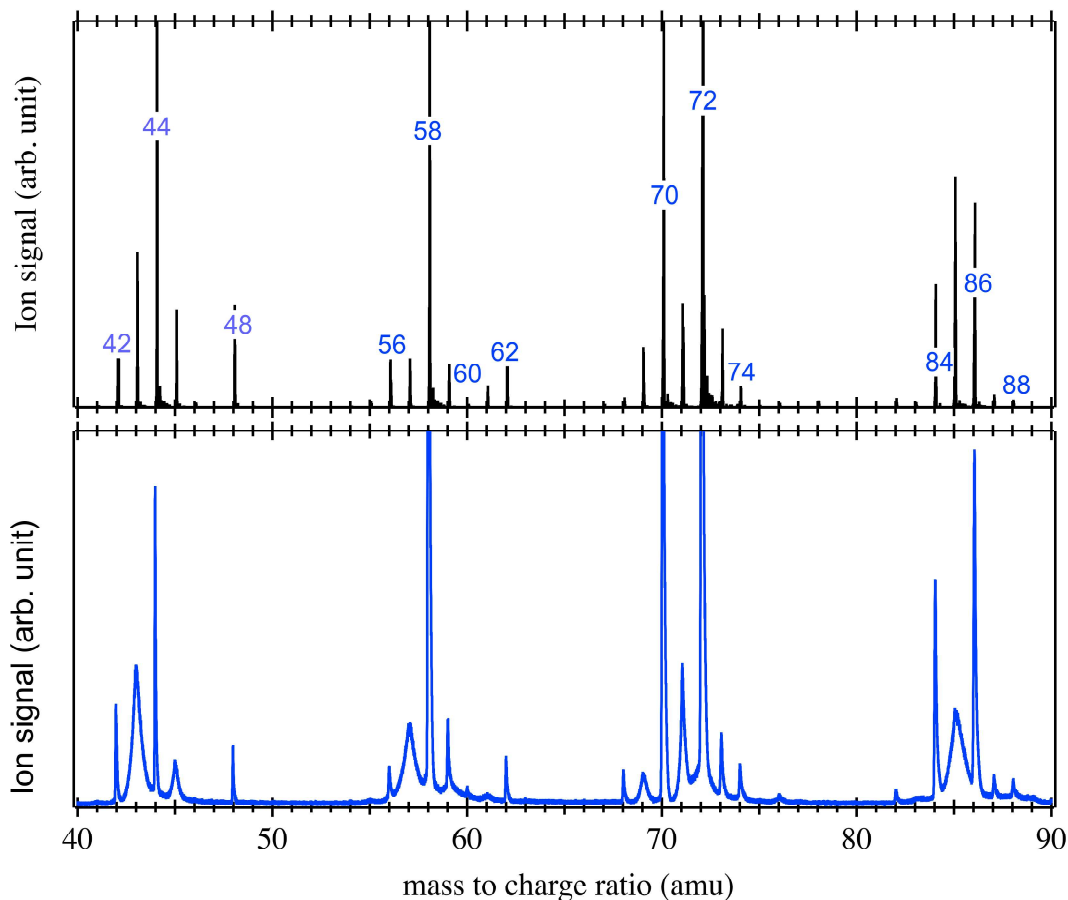


Figure 3. Comparison between (upper panel) the mass spectra obtained by SPI-MS [42] during *n*-pentane oxidation at 600 K at $\phi = 0.5$, and (lower panel) the results obtained in this work at 10.5 eV photon energy and 585 K at a similar fuel to air equivalence ratio - Peaks at m/z 58, 70 and 72 have been cut off in intensity for the sake of clarity.

Among the measured signal observed on the mass spectra, discrimination has been made between fragments and parent ions. This was easily achieved since daughter species nearly always show no structure on the corresponding TPESs because they come from unbound states of the parent ion. Additionally, the fragments exhibit broader peak shapes in the TOF-MS, due to the kinetic energy release upon fragmentation, as shown in the mass spectrum of the lower panel in the **Figure 3**. Therefore, m/z 43, 45, 57, 71 and 85 are considered as fragments even if the presence of an additional parent species for a given mass channel could not be ruled out. The origin of those fragments along with the analysis of the heaviest intense peaks above m/z 90 (such as m/z 100 and

118 present in both spectra but not shown in **Figure 3**) will be the focus of a future article and will not be considered in this work.

The identification of the important species detected in the mass spectra in **Figure 3** was attempted using their ionization energies, as summarized in **Table 2**. However, for most of the species, several identifications are possible. Therefore, the TPES corresponding to each m/z of interest should be examined more closely. The TPES related to all the m/z labeled in blue in **Figure 3** are presented and discussed hereafter in the text. These were measured during the JSR oxidation of *n*-pentane at a reaction temperature of 585 K with an equivalence ratio of $\phi = 1/3$ and 0.5.

^aprevious theoretical calculations from the literature.[22]

^bcalculated value in this work.

*NIST database (<http://webbook.nist.gov/>).

m/z	formula	Name	IE (eV)
28	C ₂ H ₄	ethylene	10.51*
	CO	carbon monoxide	14.01*
30	CH ₂ O	formaldehyde	10.88*
32	CH ₄ O	methanol	10.84*
	O ₂	oxygen (reactant)	12.07*
42	C ₃ H ₆	propene	9.73*
	C ₂ H ₂ O	ketene	9.62*
44	C ₃ H ₈	propane	10.94*
	C ₂ H ₄ O	acetaldehyde	10.23*
		ethylene oxide	10.56
	CO ₂	carbon dioxide	13.777*
48	CH ₄ O ₂	methyl hydroperoxide	9.84^a
56	C ₂ HOCH ₃	methoxyacetylene	9.48*
	C ₂ H ₃ CHO	acrolein	10.11*
58	(CH ₃) ₂ CO	acetone	9.7*
	CH ₃ CH ₂ CHO	propanal	9.96*
60	C ₂ H ₄ O ₂	acetic acid	10.69*
62	C ₂ H ₆ O ₂	ethyl hydroperoxide	9.61^a
70	C ₅ H ₁₀	1-pentene	9.49*
	C ₅ H ₁₀	2-pentene (Z)	9.01*
	C ₅ H ₁₀	2-pentene (E)	9.04*
	C ₄ H ₆ O	methyl-vinyl-ketone	9.65*
72	C ₅ H ₁₂	<i>n</i> -pentane (reactant)	10.28*
	C ₄ H ₈ O	methyl-ethyl-ketone	9.60^b
74	C ₃ H ₆ O ₂	allyl hydroperoxide	9.55^a
		propanoic acid	10.44*
84	C ₄ H ₄ O ₂	2-furanone	10.86^b
		3-furanone	9.30^b
86	C ₅ H ₁₀ O	tetrahydropyran	9.62^b
		2-methyltetrahydrofuran	9.33^b

	cis 2,4-dimethyloxetane	9.40^b
	trans 2,4-dimethyloxetane	9.38^b
	2-ethyloxetane	9.45^b
	cis 2-ethyl-3-methyloxirane	9.48^b
	trans 2-ethyl-3-methyloxirane	9.98^b
	2-propyloxirane	10.11^b
	pentanal	9.98^b
	pentenol	7.48^b
	2-pentanone	9.52^b
	3-pentanone	9.439^b
88	C₄H₈O₂	
	But-1-enyl-3-hydroperoxide	9.33^b
	But-2-enyl-1-hydroperoxide	9.52^b

Table 2. Possible identifications of species detected in SVUV-PIMS analysis using their IE. IEs are from the NIST database (<http://webbook.nist.gov/>) when available or were calculated using Gaussian (CBS-QB3 level of theory) in previous work.[22] Adiabatic IEs were calculated in this work at the PBE0/aug-cc-pVDZ(opt)/(R)CCSD(T)-F12/aug-cc-pVTZ(SP) level of theory. The identification of the compounds in bold are discussed further in the paper.

Channel m/z 42

Figure 4 displays the measured TPES for m/z 42. The observed features in **Figure 4** agree well with the literature spectra of ketene (C₂H₂O) [76] and propene (C₃H₆) [77]. The first peak corresponds to the IE of ketene at 9.62 eV and the second one at 9.73 eV to propene along with contributions corresponding to the population of the vibrational levels of the ketene cation upon ionization of the corresponding neutral. The other peaks at higher energy arise from a vibrational progression of both propene and ketene. The literature spectra were summed and weighted with appropriate factors to fit the measured PES in the appropriate photon energy range. The fit of the data results in an observed ketene:propene signal branching ratio of 1:0.5 with fit errors below 10%. Relative mole fractions could then be estimated by weighting the branching ratio using the absolute photoionization cross sections at 10.5 eV from Yang et al. [78] for ketene (24.8 Mb) and Person et al. [79] for propene (10.9 Mb). The weighting leads to a ketene:propene mole fraction (MF) ratio of 0.9:1 suggesting that propene is present in higher amounts than ketene. These results are in very good agreement with previous GC [44] and SPI-MS [42] measurements for which mole fractions of 10 ppm for ketene and of 15 ppm for propene at 580 K were determined leading to a MF ratio of ketene:propene 0.6:1. Ketene was already detected in flames [41] and JSR experiments [42] during oxidation of alkenes and alkanes, respectively. According to Bugler et al. kinetic model [44], in a JSR at low temperatures, ketene is predicted to be formed mainly by successive decomposition from the second most abundant ketohydroperoxide (the 3,1-C₅ ketohydroperoxide)

via the $\text{C}_2\text{H}_5\text{COCH}_2$ radical according to model computations. Ketohydroperoxides are the heart of the low-temperature oxidation mechanism [21] their production by two successive oxygen additions is favored as ϕ decreases. Propene is a significant product above 800 K, which can be formed by β -scission decomposition of 2-pentyl radical.

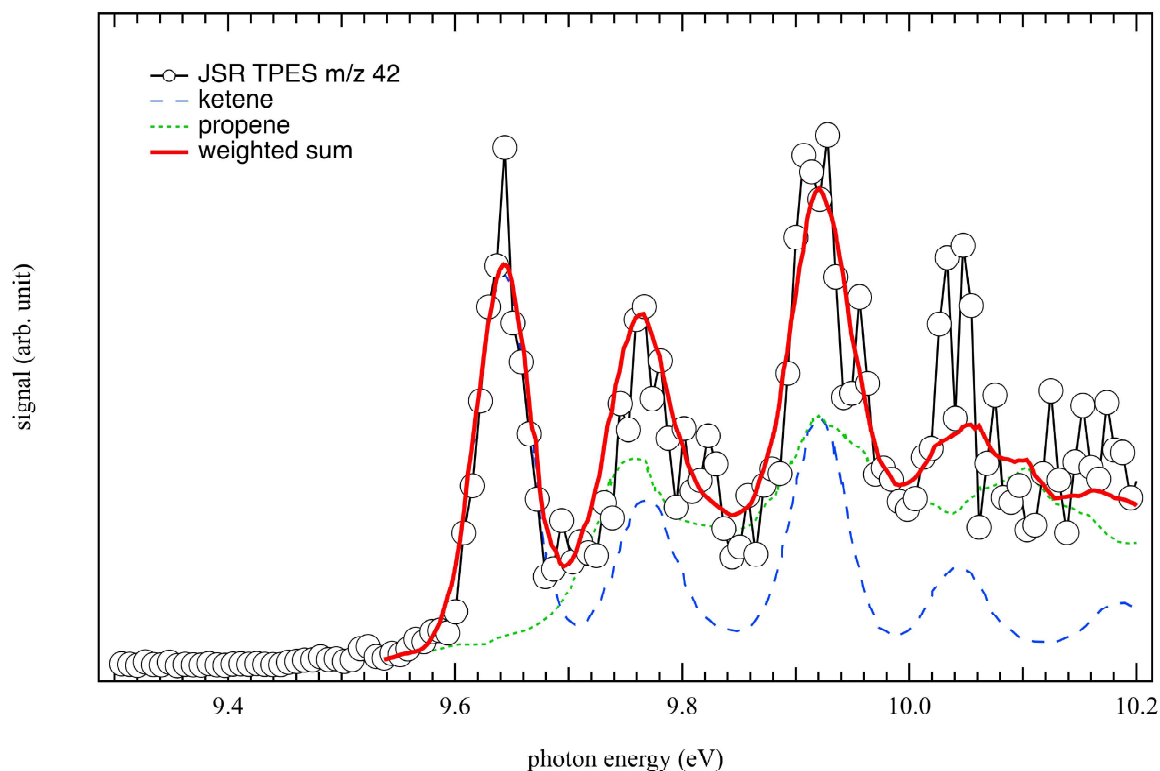


Figure 4. Comparison of the TPES at m/z 42 (open circles) measured during the JSR oxidation of n -pentane at a reaction temperature of 585 K with an equivalence ratio of $\phi = 0.5$ with the weighted sum of reference spectra using the PES of ketene (dashed red line) from Niu et al. [76] and propene (dot green line) from Bieri et al. [77] The best fit is obtained for a ketene:propene signal branching ratio of 1:0.5.

Channel m/z 44

As it is readily assigned to CH_3CHO (acetaldehyde) through its published PES [80], the TPES of m/z 44 is discussed first. For other m/z , several species assignments can be proposed. The experimental TPES of m/z 44 is shown in **Figure 5**, and. Another possible isomer could be ethylene oxide $\text{C}_2\text{H}_4\text{O}$ based on its ionization energy (IE: 10.56 eV). However, there is nothing

evident at this photon energy to suggest its presence, and the reported reference PES [81] for this species in the literature does not match the bands seen in **Figure 5**. Propane (C_3H_8) is another possibility with an IE of 10.94 eV [82], but the reported TPES does not match the bump seen around 11 eV in our TPES and GC experiments show that propane can only be formed at much higher temperatures. Therefore, we did not see propane in TPES obtained at 585K and the unsigned bands peaking at 10.9 eV and 11.3 eV cannot be matched to other isomeric structures and might arise from dissociative ionization of heavier species. Note that carbon dioxide cannot be detected in this photon energy range since its ionization energy is much higher at 13.77 eV. Acetaldehyde (IE: 10.229 eV) [83] is a toxic pollutant and a major intermediate during alkane low-temperature oxidation arising mainly from the decomposition of the major ketohydroperoxide (the 2,4- C_5 ketohydroperoxide) according to model computations. The mole fraction of acetaldehyde at 580 K ($\phi = 0.5$) measured by GC [44] is 600 ppm, while that of ethylene oxide is 15 ppm supporting the lack of signal around its predicted IE.

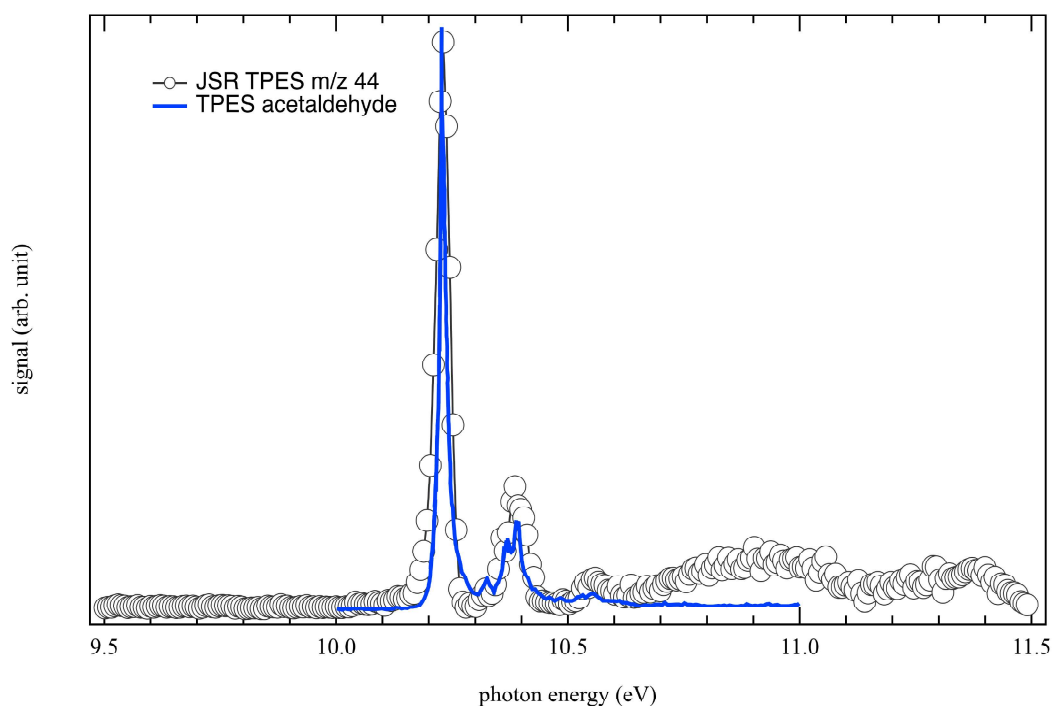


Figure 5. Comparison between the TPES at m/z 44 (open circles) measured during the JSR oxidation of *n*-pentane at a reaction temperature of 585 K with an equivalence ratio of $\phi = 1/3$ and the TPES of acetaldehyde (blue line) from Yench et al. [84].

Channel m/z 48

The TPES correlated to 48 amu is displayed in **Figure 6**. It shows a threshold around 9.8 eV, which is in good agreement with previous experimental and theoretical ionization energy of methyl hydroperoxide CH_3OOH (IE: 9.84 eV) in the literature.[42] However no theoretical or experimental PES are available in the literature. Methyl hydroperoxide (mole fraction of 150 ppm at 585 K, $\phi = 0.5$) was found along with H_2O_2 , the most abundant peroxide in SVUV-PIMS experiments during the oxidation of *n*-pentane.[42] Note that the sharp signal drop around 11 eV is due to ion fragmentation as in **Figure 9**.

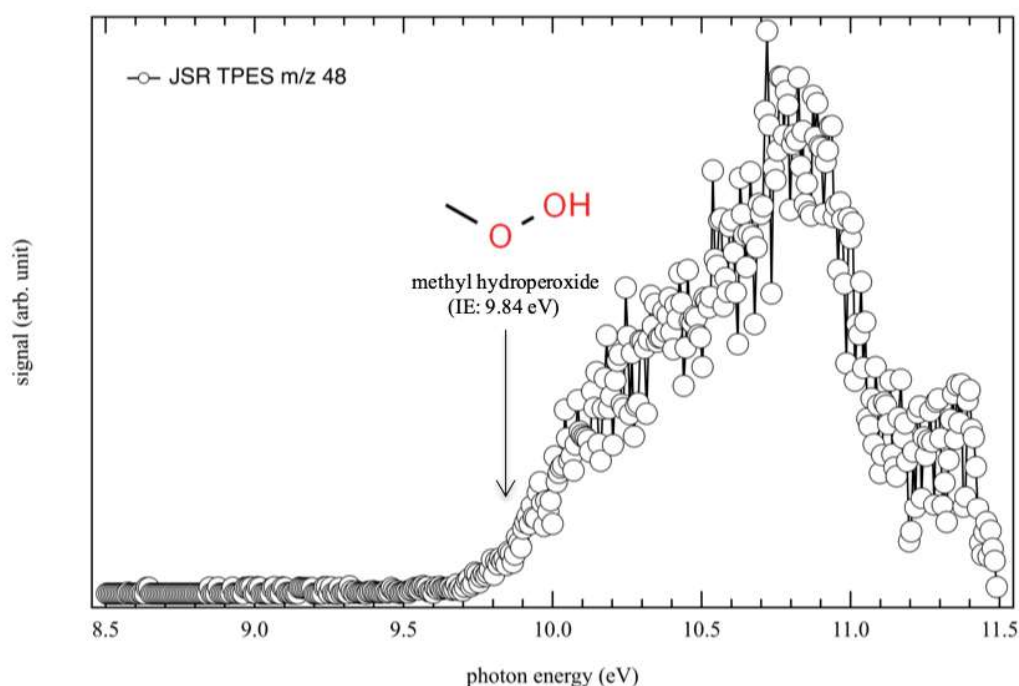


Figure 6. Measured TPES at m/z 48 (open circles) during the JSR oxidation of *n*-pentane at a reaction temperature of 585 K with an equivalence ratio of $\phi = 1/3$.

Channel m/z 56

Figure 7 shows the experimental TPES at m/z 56 measured in JSR which could come from potential contributions from several species such as C_4H_8 (but-2-ene, iso-butene, but-1-ene) and $\text{C}_3\text{H}_4\text{O}$ isomers (acrolein ($\text{C}_2\text{H}_3\text{CHO}$), methylketene, methoxyacetylene (C_2HOCH_3)) isomers. However, methylketene (IE: 8.95 eV) [85], but-2-ene (IE: *trans* 9.10 & *cis* 9.11 eV) and iso-butene

(IE: 9.22 eV) (<http://webbook.nist.gov/>) could be easily ruled out based on their lower ionization energies and compared to the threshold observed around 9.4 eV in **Figure 7**. The best fit obtained from the available PESs of acrolein, methoxyacetylene, and but-1-ene is shown in **Figure 7**. This fit is for an observed acrolein:methoxyacetylene:but-1-ene signal branching ratio of 1:0.04:0.08 and allows us to infer that the measured spectrum is dominated by acrolein (IE: 10.11 eV) [84]. The unsaturated C₃ aldehyde, acrolein is a very toxic compound and also a typical intermediate found during the oxidation of organic fuels at low temperature.[86] Acrolein was measured in relatively high amounts during *n*-pentane oxidation experiments (around 180 ppm at 580 K and $\phi=0.5$) [44]. Acrolein, the formation of which is satisfactorily predicted by the model (140 ppm), can be obtained through fast decomposition of allyl hydroperoxide, obtained by the combination of the abundant allyl and HOO radicals. However, the best fit does not reproduce satisfactorily the low photon energy part of the spectrum. Despite the fact that the weighting factor error on acrolein is around 3%, the weighting factor errors on methoxyacetylene and but-1-ene are 40% and 10% respectively due to a low signal to noise ratio. Thus, it is not possible to address or rule out their respective contribution in this work but if so, they are formed as minor species. Methoxyacetylene (IE: 9.48 eV) [87] is not considered in the *n*-pentane oxidation model of Bugler et al. [44] and under the present conditions, butenes were also measured in low amount by GC [44] (7 ppm). However, but-1-ene (IE: 9.55 eV) [88] is a significant product above 800 K because it can be formed by C-C β -scission decomposition of the 3-pentyl radical.

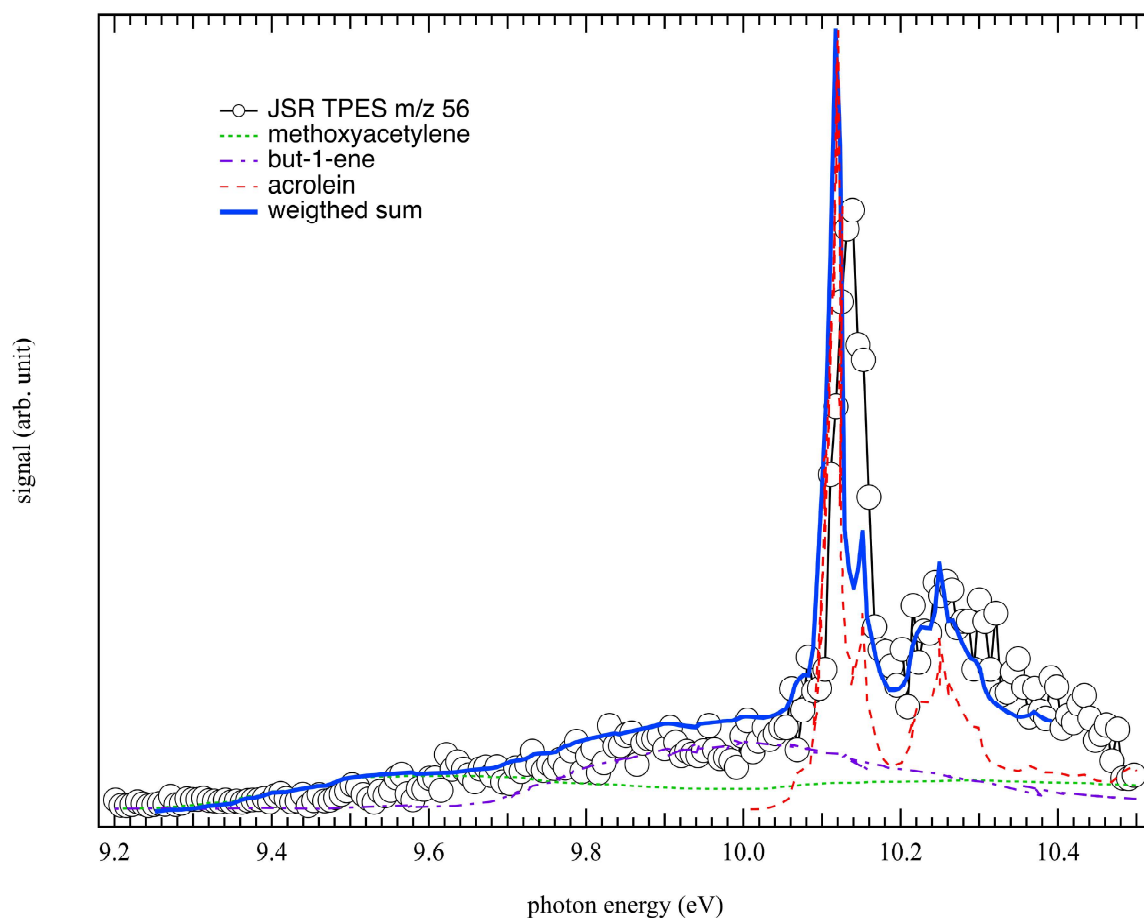


Figure 7. Comparison between the TPES at m/z 56 (open circles) measured during the JSR oxidation of *n*-pentane at a reaction temperature of 585 K with an equivalence ratio of $\phi = 0.5$ and the weighted sum of reference spectra using the TPES of acrolein (dashed red line) from Yench et al. [84], and the PES of methoxyacetylene (dot green line) [87], and but-1-ene (dot-dashed line) [88]. The best fit is obtained for a acrolein:methoxyacetylene:but-1-ene signal branching ratio of 1:0.04:0.08.

Channel m/z 58

Figure 8 shows the TPES of m/z 58, the second highest peak in the TOF-MS spectra of **Figure 3**, as measured in JSR. It appears to be nicely reproduced by a mixture of reference spectra of acetone [89] and propanal [90]: the first two peaks correspond to acetone (IE: 9.7 eV) [91] while the third one to a contribution from both acetone and propanal (IE: 9.96 eV) [78]. Other potential isomers at this mass channel such as methyloxirane would lead to a threshold at 10.22 eV for

which almost no signal is observed. [92] The fit to the data returns an observed acetone:propanal signal branching ratio of 1:0.1 corresponding to a acetone:propanal 1:0.12 mole fraction ratio using the absolute photoionization cross sections at 10.5 eV from Wang et al. [93] for propanal (9.51 Mb) and from Cool et al. [94] for acetone (11.20 Mb). This result is at odds with the GC measurements at 600K [44], where acetone was found in amounts 100 times lower than propanal (mole fraction = 120 ppm at 580 K, $\phi = 0.5$). This unfavorable ratio is, to a lower extent, confirmed by the model, which predicts twice more propanal (3.6×10^{-4}) than acetone (1.7×10^{-4}).

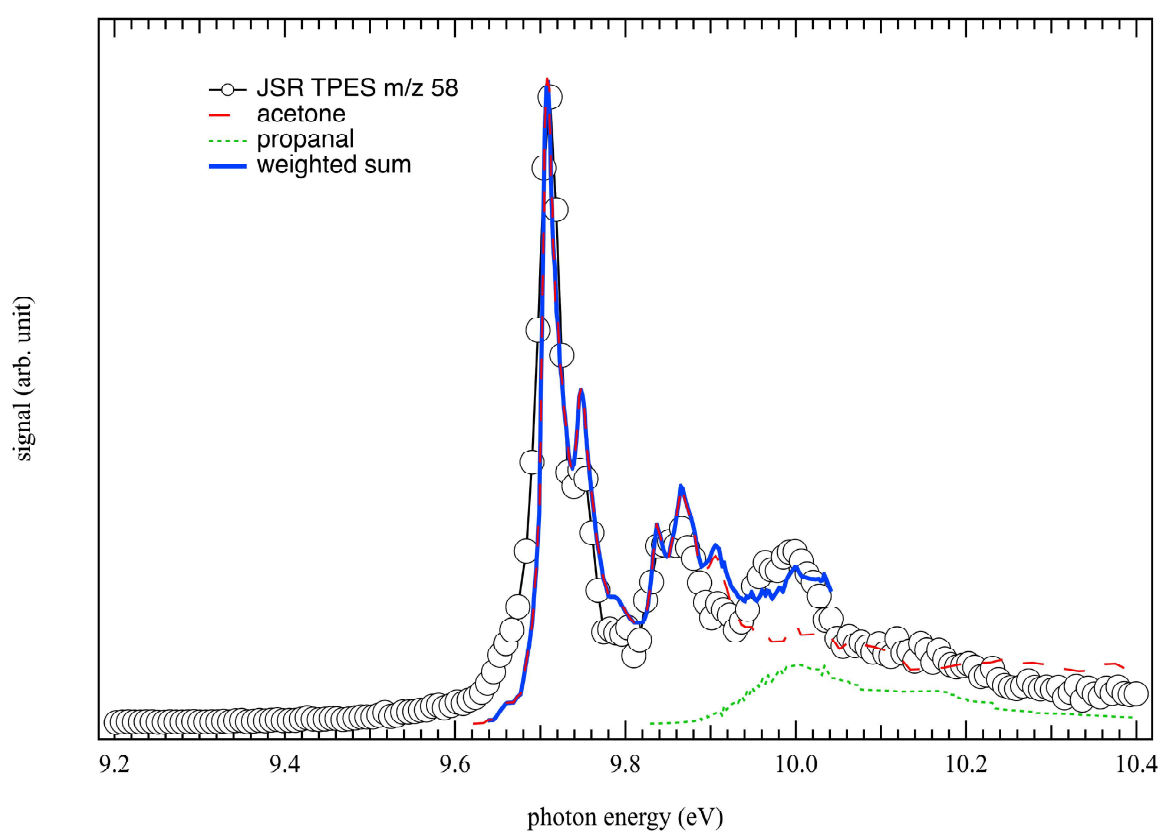


Figure 8. Comparison between the measured TPES at m/z 58 (open circles) measured during the JSR oxidation of *n*-pentane at a reaction temperature of 585 K with an equivalence ratio of $\phi = 0.5$ and the weighted sum of reference spectra using the PES of acetone (dashed red line) from Dannacher & Stadelmann [89] and propanal (dot green line) from Rennie et al. [90] The best fit is obtained for an acetone:propanal branching ratio of 1:0.1.

To check if the signal at m/z 58 is not due to the use of acetone as cleaning solvent in the experiments, **Figure S1** displays its variation of the ion signal at m/z 58 as function of the temperature, showing well a product profile, negligible below 540 K and increasing with temperature. Propanal, the mole fraction of which is correctly enough predicted, is formed through the decomposition of the 3-pentylhydroperoxide. Acetone can be easily formed by H-abstractions by CH_3COCH_2 , the radical arising, together with acetaldehyde, from the decomposition of the major ketohydroperoxide (the 2,4- C_5 ketohydroperoxide). However, the predicted formation of acetone is very low in the n -pentane oxidation model of Bugler et al. [44]. This is because many important possible H-abstractions by this radical to give acetone are not considered in the model. This is especially the case of the H-abstractions with the fuel or with aldehydes.

Channel m/z 60 and m/z 62

Figure 9 displays the experimental TPES of m/z 60, which is in very good agreement with the experimental PES of acetic acid (CH_3COOH) from von Niessen et al. [95], although with a better resolution here. The formation of acetic acid (IE: 10.65 eV) and other organic acids in low-temperature oxidation of n -alkanes are explained with the Korcek mechanism, pathways based on the ketohydroperoxide decomposition via a cyclic peroxide isomer.[96] Acetic acid has been detected by SVUV-PIMS [42] and quantified by GC measurements [44] as the major acid produced during low temperature oxidation of n -pentane, with a mole fraction of 40 ppm at 600 K and $\phi = 0.5$. **Figure 9** also shows the presence of a compound at m/z 62 during JSR experiments, which has been identified as ethylhydroperoxide ($\text{C}_2\text{H}_5\text{OOH}$) based on its calculated IE (9.61 eV) and quantified (mole fraction of 50 ppm at 580 K, $\phi = 0.5$) in a previous n -pentane oxidation study. [42] Along with methylhydroperoxide attributed to the signal at m/z 48, they are the two major alkylhydroperoxides mainly produced through HOO radicals combining with alkyl peroxy radicals in low-temperature lean fuel environment. Note that the slow rise observed is probably due to some geometry change between the neutral and the cation leading to poor FC factors, so that the adiabatic and vertical IEs are very different. Such a situation makes the PES more sensitive to hot band contribution, probably explaining the methyl and ethylhydroperoxide signals below their respective IE.

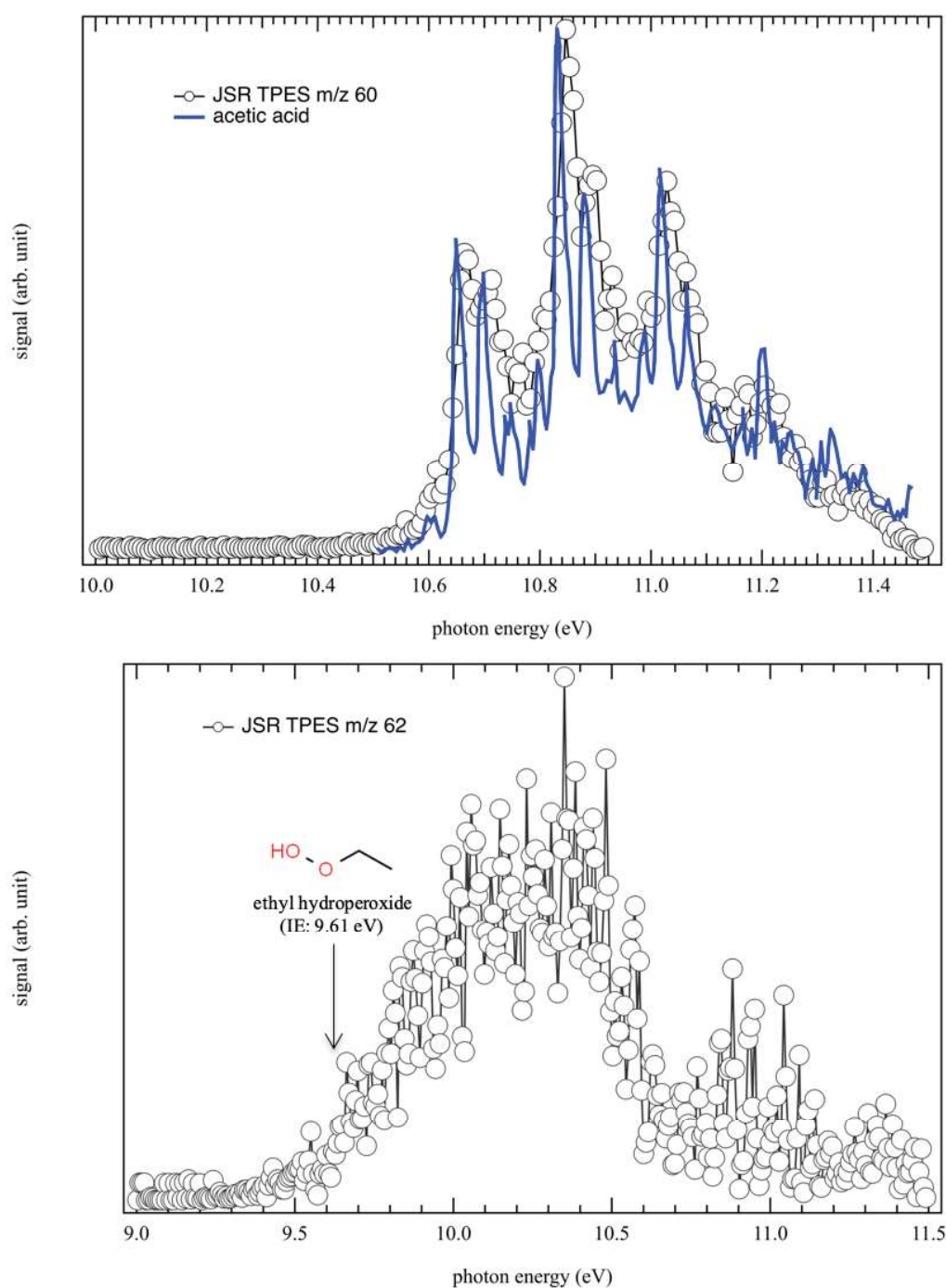


Figure 9. (Upper panel) comparison between the measured TPES at m/z 60 (open circles) measured during the JSR oxidation of *n*-pentane at a reaction temperature of 585 K with an equivalence ratio of $\phi = 1/3$ and the integrated TPES of acetic acid (blue line) from von Niessen et al.[95] (Lower panel) Measured TPES at m/z 62 (open circles) measured during the JSR oxidation of *n*-pentane at a reaction temperature of 585 K with an equivalence ratio of $\phi = 1/3$.

Channel m/z 70

As the molecular mass increases, more and more potential candidates and isomers have to be considered and *a priori* choices based on chemical knowledge need to be made. This is the case of the m/z 70 corresponding photoelectron spectra displayed in **Figure 10**. At m/z 70 based on *n*-pentane molecular structure, linear isomers such as 1-pentene (IE: 9.5 eV) and 2-pentene (IE: 9.04 eV) are most likely to be formed compared to branched structures, such as 2-methyl-1-butene (IE: 9.1 eV), 2-methyl-2-butene (IE: 8.69 eV) and 3-methyl-1-butene (IE: 9.5 eV).[40]. Indeed, 2-methyl-2-butene can already be ruled out due to its low IE with respect to our TPES signal rise. The PES 3-methyl-1-butene [40] is very similar to that of 1-pentene, and the PES of 2-methyl-1-butene has been recently calculated taking into account possible rotamers [40] but its vibronic structure, although close to that of 2-pentene, does not match the present TPES. Based on the molecular structure argument enounced before, and the fact that 2-methyl-2-butene can be excluded, we have not considered neither 3-methyl-1-butene nor 2-methyl-1-butene in the fitting procedure. In addition, oxygenated species such as methyl vinyl ketone C_4H_6O (IE: 9.65 eV) could also contribute significantly to the signal measured at m/z 70.[97] The shape of the measured TPES of m/z 70 displayed in **Figure 10** is very well reproduced from the weighted contributions of three different isomers (2-pentene, 1-pentene and methyl vinyl ketone) with an observed 2-pentene:1-pentene:methyl vinyl ketone signal branching ratio of 1:0.3:0.6. The quality of the fit further validates the choice of removing the branched isomers. Under the GC conditions [44], 1-pentene was detected in peak mole fractions sometimes over ten times those of 2-pentene due to potential co-elution with the reactant. However, simulations indicate a 2.6 times higher mole fraction of 2-pentene (170 ppm) compared to that of 1-pentene (65 ppm). According to Bugler et al. model [44], pentenes are mainly formed from HOO elimination from the three pentylperoxy radicals derived from the three (one primary and two secondary) pentyl radicals. 2-pentene arises only from the more abundant secondary pentyl radicals, while 1-pentene arises from both one primary and one secondary pentyl radicals. The mole fraction (580 K, $\phi = 0.5$) of methyl vinyl ketone (17 ppm) was found to be about a third of that of pentenes [44] through GC measurements, which is in agreement with the present results assuming similar absolute ionization cross-sections for the three isomers. Methyl vinyl ketone is not considered in the model. [44]

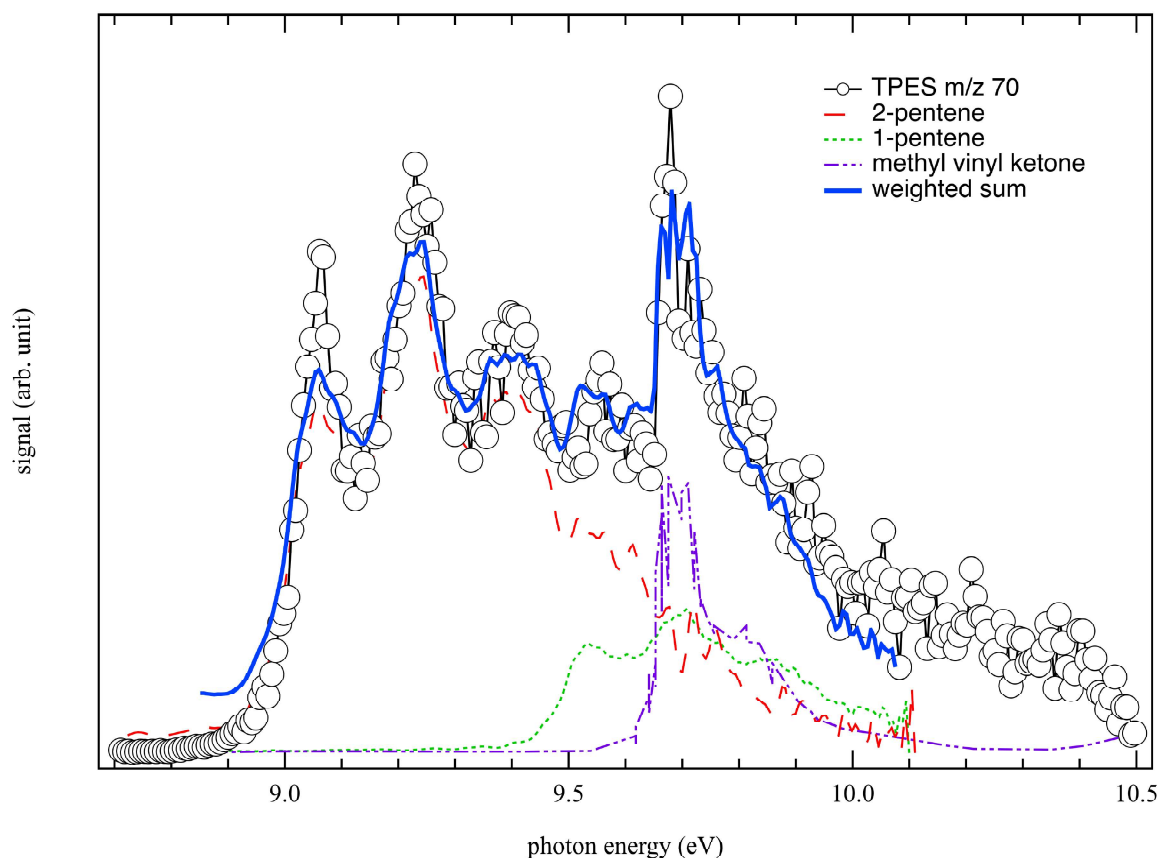


Figure 10. Comparison of the measured TPES at m/z 70 (open circles) obtained in the JSR during n -pentane oxidation at a reaction temperature of 585 K with an equivalence ratio of $\phi = 0.5$ to the weighted sum of reference spectra using the PES of 2-pentene (dashed red line) and 1-pentene (dot green line) from Pieper et al. [40] and methyl vinyl ketone (purple dot-dashed line) from Tam et al. [98] The best fit is obtained for a 2-pentene:1-pentene:methyl vinyl ketone signal branching ratio of 1:0.3:0.6.

Channel m/z 72

Figure 11 displays the experimental TPES of m/z 72, which is in very good agreement with the experimental PES of Methyl Ethyl Ketone (MEK) from Pieper et al. [40], although with a better resolution here. We observe a double structure around 9.6 eV, as verified by the simulated TPES of MEK (IE: 9.6 eV) also displayed in **Figure 11**. Numerous additional potential isomasses at this mass channel were ruled out such as iso-butanol, tetrahydrofuran, 2-methoxypropene, ethyl vinyl ether, 3-buten-1-ol, 3-buten-2-ol and *iso*-butanal. For instance, 2-methoxypropene (IE: 8.64

eV) and ethyl vinyl ether (IE: 8.98 eV) are ruled out based on their respective ionization energies, which sit below the rise of the TPES signal. The other isomasses: *n*-butanal, iso-butanol, tetrahydrofuran, 3-buten-1-ol, 3-buten-2-ol and iso-butanal are dismissed on the basis of their PES, which do not match the experimental TPES (cf. **Figure S2**). [40] This result is in agreement based on *n*-pentane molecular structure, where contributions from branched structures such as *iso*-butanol (IE: 9.24 eV), 3-buten-1-ol (IE: 9.56 eV), 3-buten-2-ol (IE: 9.53 eV) and iso-butanal (IE: 9.83 eV) are expected to be small. The mole fraction of Methyl Ethyl Ketone (MEK) was measured equal to 90 ppm at 580 K ($\phi = 0.5$) in previous GC experiments [44], with that of butanal being 5 times lower (18 ppm under the same conditions). The much lower concentration of the butanal isomer is consistent with the lack of signal in the present results assuming comparable photoionization cross sections. MEK (predicted mole fraction = 3 ppm) is modeled as being formed by H-abstractions from the $C_2H_5COCH_2$ radical obtained from the decomposition of the second most abundant ketohydroperoxide (the 3,1- C_5 ketohydroperoxide); here also only many H-abstractions with $C_2H_5COCH_2$ radical are missing in the model [44] involving a probable significant underprediction. It should be noted that the peak at 9.54 eV, which is also clearly seen in the experimental PES measured by Pieper et al. [40], is not seen in the calculations using a vibrational temperature of 0K so it must likely come from a hot band because the high temperature at which this compound is formed.

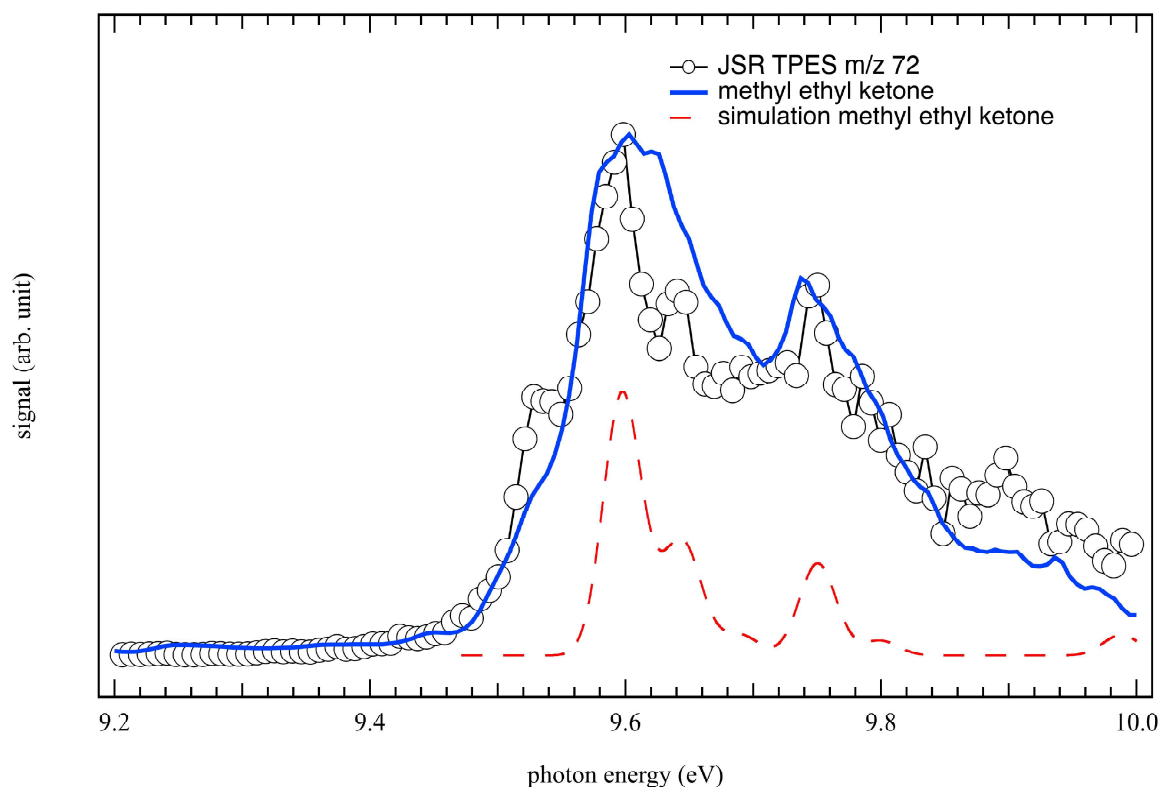


Figure 11. Comparison of the measured TPES at m/z 72 (open circles) obtained in the JSR during n -pentane oxidation at a reaction temperature of 585 K with an equivalence ratio of $\phi = 0.5$ to the reference spectrum of MEK (solid blue line) from Pieper et al. [40] and the envelope from convolution of the FC factors for the MEK (long dashed red line) as computed in this work at the PBE0/aug-cc-pVDZ level and shifted to fit with the adiabatic ionization energy determined at the PBE0/aug-cc-pVDZ(opt)/(R)CCSD(T)-F12/aug-cc-pVTZ(SP) level. Note that for the sake of clarity, the signal above 10.1 eV is not shown since it is saturated by the n -pentane signal (IE: 10.28 eV).

Channel m/z 74

The TPES shown in **Figure 12** (m/z 74 corresponding to a minor peak in **Figure 3**) could correspond to allyl hydroperoxide (IE: 9.55 eV), the lightest alkenyl hydroperoxide, and propanoic acid (IE: 10.44 eV). The organic acid was measured in significant amounts during the oxidation of several alkanes at low temperatures in the past.[47] Regarding allyl-OOH, it was already detected in SVUV-PIMS and SPI-MS experiments (mole fraction of 7 ppm at 580 K ($\phi =$

0.5)).[42,44] Allyl hydroperoxide (predicted mole fraction = 2 ppm) is mainly formed by combination of allyl and HOO radicals.

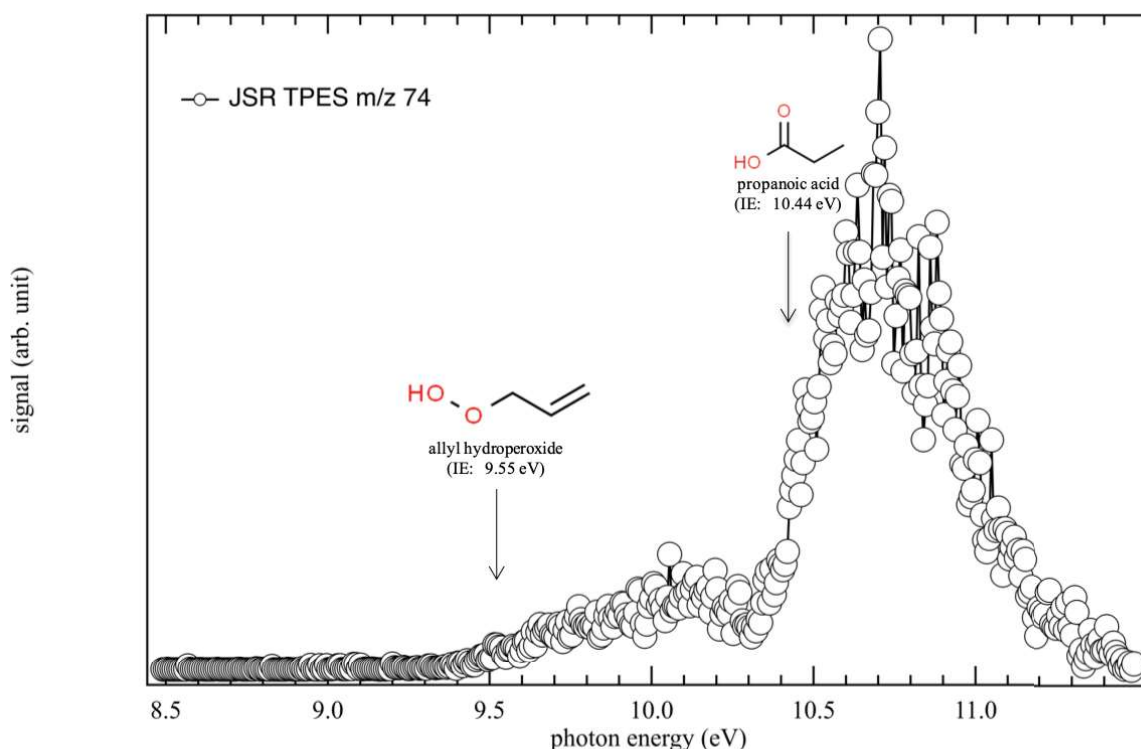


Figure 12. Measured TPES at m/z 74 (open circles) obtained in the JSR during *n*-pentane oxidation at a reaction temperature of 585 K with an equivalence ratio of $\phi = 1/3$.

Channel m/z 84

Figure 13 shows the measured TPES at m/z 84 (open circles) obtained in the JSR during *n*-pentane oxidation. GC-MS experiments [44] led to suggest pentenones for this m/z but with a slightly higher start of detection, from 590 K instead of the 585K used to record the TPES. This would be consistent with previous measurements in SVUV-PIMS during *n*-heptane oxidation at low temperature suggesting the possible formation of products derived from cyclic ethers such as furanones (C₄H₄O₂) [22] with the potential formation of at least two products contributing to this mass channel such as 3-furanone (IE: 9.30 eV) and 2-furanone (IE: 10.86 eV). Based on the good overlap between the measured TPES and the envelope from convolution of the FC factors for the 3-furanone, we are able to pinpoint the formation of 3-furanone and rule out the other furanone

isomer for which the TPES in **Figure 13** shows no measurable intensity at its ionization energy. Contribution from hydrocarbons at this mass such 1-hexene (C_6H_{12}) could also be ruled out based on the shape of its PES, since there is a second, intense electronic band starting above 10.2 eV [99] which we don't see in our TPES. Furanones are not considered in the model, but are expected to derive from dihydrofurans by H-abstraction followed by a combination with HO_2 radicals and the decomposition of the obtained hydroperoxides. 2,3-dihydrofuran is considered in the model, but it is predicted to be formed in very negligible amounts.

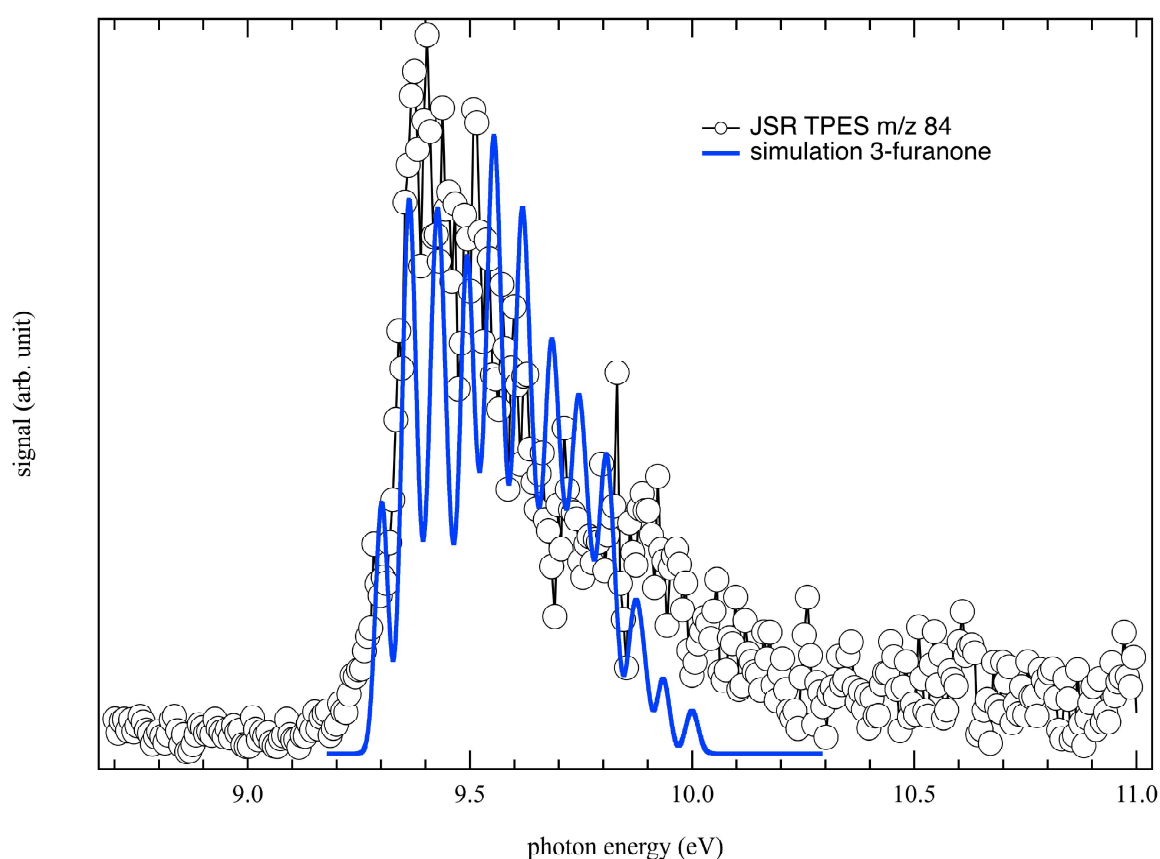


Figure 13. Measured TPES at m/z 84 (open circles) obtained in the JSR during *n*-pentane oxidation at a reaction temperature of 585 K with an equivalence ratio of $\phi = 1/3$ and the envelope from convolution of the FC factors for the 3-furanone (blue line) as computed at the PBE0/aug-cc-pVDZ level and shifted to fit with the adiabatic ionization energy determined at the PBE0/aug-cc-pVDZ(opt)//(R)CCSD(T)-F12/aug-cc-pVTZ(SP) level.

Channel m/z 86

Figure 14 displays the TPES obtained for the intense m/z 86 peak and the simulated TPES of 2-methyltetrahydrofuran (IE: 9.33 eV), 2-pentanone (IE: 9.52 eV), 3-pentanone (IE: 9.439 eV), cis 2-ethyl-3-methyloxirane (IE: 9.48 eV), trans 2,4-dimethyloxetane (IE: 9.38 eV) and 2-ethyloxetane (IE: 9.45 eV) to fit the TPES. The best fit is obtained for a 2-methyltetrahydrofuran:2-pentanone:3-pentanone:cis 2-ethyl-3-methyloxirane:trans 2,4-dimethyloxetane:2-ethyloxetane observed signal branching ratio of 0.69:0.82:1:0.82:0.56:0.39. Numerous additional potential isomers at this mass channel were ruled out based on previous studies in GC-MS [44]. All the $C_5H_{10}O$ isomers for m/z 86 with an amount below 10 ppm have not been considered in the fitting procedure: trans 2-ethyl-3-methyloxirane, pentanal, pentenol and 2-propyloxirane and tetrahydropyrans (see **Table S1**). The cis conformation of 2,4-dimethyloxetane was not considered since the IE with the trans conformation is close (trans: 9.38 eV and cis: 9.40 eV) and the experimental resolution does not allow to differentiate their respective contributions. To obtain the relative contribution of the 6 other isomers for m/z 86, calculated TPES of 2-methyltetrahydrofuran, 2-pentanone, 3-pentanone, cis 2-ethyl-3-methyloxirane, trans 2,4-dimethyloxetane and 2-ethyloxetane were considered in the evaluation. The fitting procedure sums and weights with 6 appropriate factors the calculated TPES of the 6 isomers in the appropriate photon energy range. The best fit displayed in **Figure 14** reproduces satisfactorily the overall structure of the measured TPES of m/z 86 from the weighted contributions of the different isomers. **Table S1** reports the comparison between the amount detected by GC-MS [42], the predicted value using the model of Bugler et al. [44] and the observed signal branching ratio for isomers at m/z 86.

However, the evaluation faces some challenges here since the calculated TPES of the isomers overlap in a narrow energy region. Thus, with the noise level for the signal at this mass channel, the relative contribution of the different isomers must be interpreted with care, and the uncertainty in the observed signal branching ratio is associated with the experimental TPES fit. As shown in **Figure S3**, the procedure is more sensitive to non-overlapping and structured PES, such as trans 2,4-dimethyloxetane (isolated on the low energy part) or 2-methyltetrahydrofuran (double band structure). Overall, the systematic errors on the branching ratios range from a few percent for the abovementioned isomers, to a few tens of percent that sometimes exceed the fitted value itself.

The evaluation shows the formation of several linear and cyclic isomers. Cyclic ethers are involved in the low temperature gas phase oxidation of different types of fuels, emitted in exhaust gases of engines from an incomplete combustion. They derived from an oxygen addition on an alkyl radical (deriving from the reactant) to form a peroxy radical ROO followed by several isomerization steps to yield a hydroperoxy alkyl radical QOOH, which could decompose to form three, four, five and six membered ring cyclic ethers. Usually, the five membered ring cyclic ethers (tetrahydrofurans and oxolanes) are expected to be the most abundant during low-temperature oxidation of linear *n*-alkanes due to a lower ring strain energy involved in the transition state during the isomerization in comparison to that of the other cyclic transition states.[100] The presence of 2-methyltetrahydrofuran (2-MeTHF) in this work along with the 88.4 ppm mole fraction measured in previous GC experiments at 580 K ($\phi = 0.5$) [44] supports this statement. However, the evaluation in this work does not conclude on the dominance of 2-MeTHF due to lack of information on photoabsorption cross sections in the literature. The formation of four membered ring cyclic ethers (oxetanes) is usually observed but these species are present in much smaller amounts than five membered ring ones. The evaluation revealed the formation of 2,4-dimethyloxetane and 2-ethyloxetane. Both species were detected as major species during previous GC experiments [44] with a mole fraction equal to 16.3 and 19.6 ppm at 580 K ($\phi = 0.5$) respectively. Cis 2-ethyl-3-methyloxirane is also detected which is consistent with the 22.4 ppm mole fraction measured in previous GC experiments [44] at 580 K ($\phi = 0.5$) even if three membered ring cyclic ethers are not easily detected due to a difficult isomerization with a high extra internal energy transition state. Finally, the evaluation addressed the contribution of two linear ketone isomers: 2- and 3-pentanone which was found as the second major species after 2-MeTHF in previous GC experiments during low temperature *n*-pentane oxidation [44] with a mole fraction equal to 54 ppm at 580 K ($\phi = 0.5$). Those species are formed from H-abstraction reactions from alkyl radicals with a carbonyl group leading to the formation of ketones such as acetone or pentanone. According to Bugler et al model [44], 2- and 3-pentanone arise, respectively, from 2- and 3-pentylperoxy radicals by reaction with methyl-/ethyl-peroxy radicals producing these ketones, methanol/ethanol and O₂.

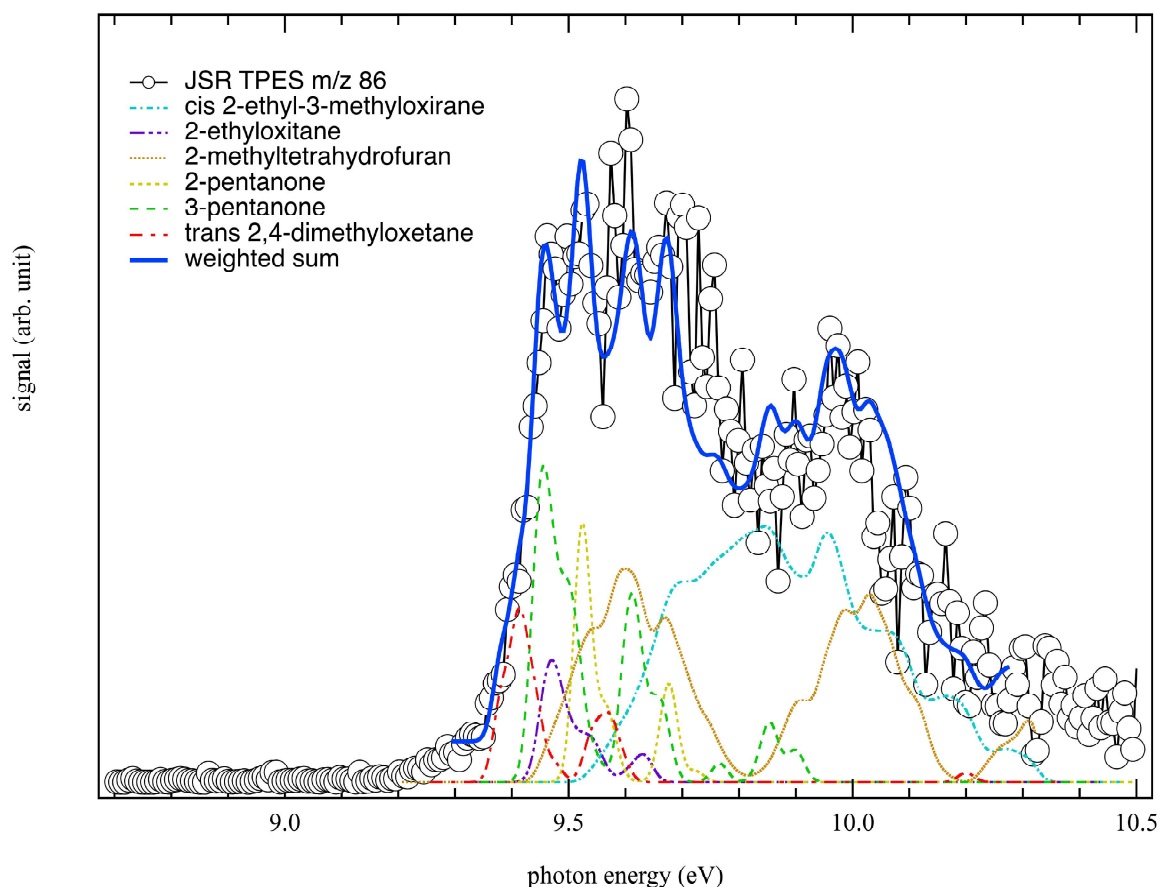


Figure 14. Comparison of the measured TPES at m/z 86 (open circles) obtained in the JSR during n -pentane oxidation at a reaction temperature of 585 K with an equivalence ratio of $\phi = 0.5$ to the weighted sum of the envelopes from convolution of the FC factors for the 2-methyltetrahydrofuran (orange small dotted line), 2-pentanone (yellow long dotted line), 3-pentanone (green short dashed line), cis 2-ethyl-3-methyloxirane (cyan dot-dashed line), trans 2,4-dimethyloxetane (red long and short dashed line) and 2-ethyloxetane (purple long line followed by two short dashes) as computed at the PBE0/aug-cc-pVDZ level and shifted to fit with the adiabatic ionization energy determined at the PBE0/aug-cc-pVDZ(opt)/(R)CCSD(T)-F12/aug-cc-pVTZ(SP) level. The best fit is obtained for a 2-methyltetrahydrofuran:2-pentanone:3-pentanone:cis 2-ethyl-3-methyloxirane:trans 2,4-dimethyloxetane:2-ethyloxetane observed signal branching ratio of 0.69:0.82:1:0.82:0.56:0.39.

Channel m/z 88

Figure 15 displays the TPES at m/z 88 obtained in the JSR during *n*-pentane oxidation and the envelope from convolution of the FC factors for the but-1-enyl-3-hydroperoxide. During previous alkane oxidation experiments using TOF-MS combined with tunable synchrotron photoionization and during GC analysis (0.02 ppm at 580 K) [42,44] the formation of C₄ alkenylhydroperoxides was suggested along with butanoic acid but without further information on the identification of the isomer of C₄ alkenylhydroperoxides. In this work, FC analysis allow us to observe a good overlap between the measured TPES at m/z 88 and the envelope from convolution of the FC factors for the but-1-enyl-3-hydroperoxide (IE: 9.33 eV). The convolution of the simulated vibrationally resolved electronic spectrum of the other isomer but-2-enyl-1-hydroperoxide (IE: 9.52 eV) and displays in the **Figure 15** allows us to rule out its contribution in the measured signal at mass channel 88. The formation of butanoic acid is also ruled out since no signal was observed at its ionization energy, 10.3 eV. It should be noted that the large difference in shape between the TPES and the simulations is explained by the fact that when high masses are reached, there are more internal modes, especially low frequencies, that may be populated prior to photon ionization contributing to the spectra as hot bands. Also several conformers may be formed and may contribute. These effects are not taken into account in the simulated spectra.

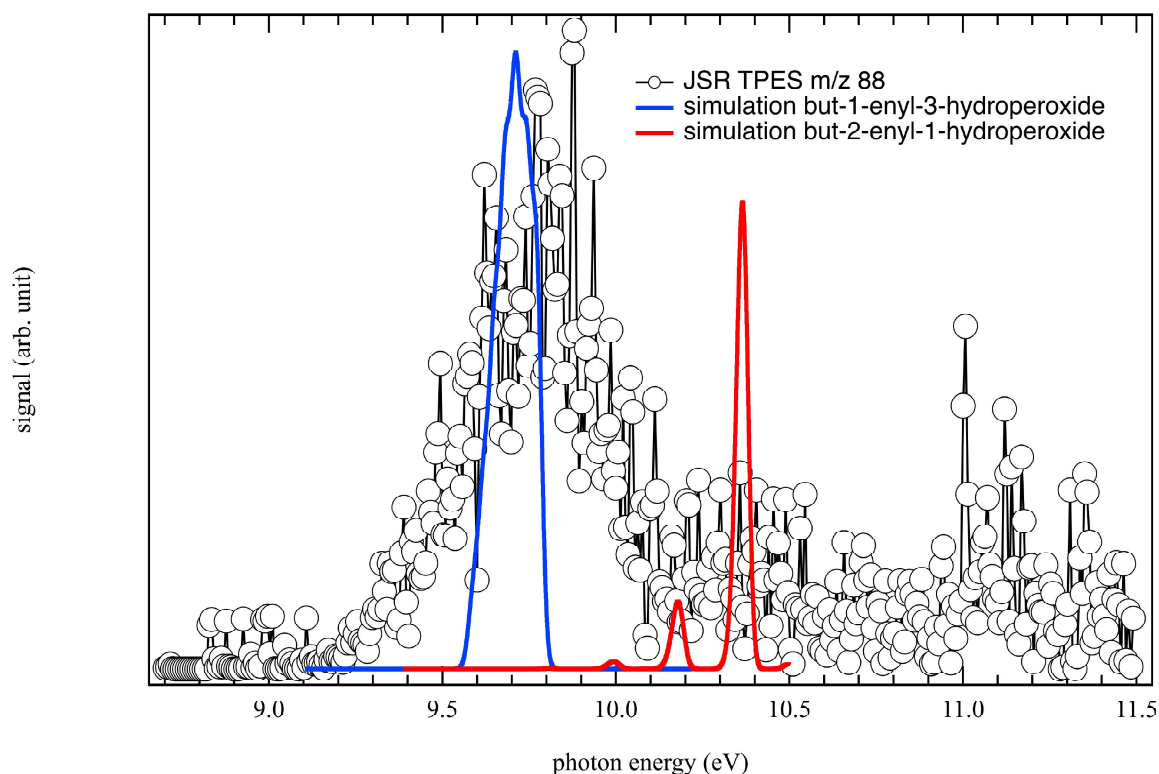


Figure 15. Measured TPES at m/z 88 (open circles) obtained in the JSR during *n*-pentane oxidation at a reaction temperature of 585 K with an equivalence ratio of $\phi = 1/3$ and the envelope from convolution of the FC factors for the but-1-enyl-3-hydroperoxide (blue line) and the but-2-enyl-1-hydroperoxide (red line) at as computed at the PBE0/aug-cc-pVDZ level and shifted to fit with the adiabatic ionization energy determined at the PBE0/aug-cc-pVDZ(opt)//(R)CCSD(T)-F12/aug-cc-pVTZ(SP) level.

4. Summary and conclusions

The oxidation of *n*-pentane has been studied in a JSR, for the first time using the *i*²PEPICO spectroscopy technique for the analysis of combustion intermediates. The *i*²PEPICO approach reveals the fingerprint TPES of each species, allowing specific information about the chemical composition at a given mass channel to be unraveled. Especially in combustion environments such as in a JSR, this technique is advantageous to decipher the contribution of several isomers with close ionization energies and when the slopes of the PIE are featureless. When coupled to FC calculations, this method allows the determination of the vibrational temperature of the environment by comparing the intensity ratio between the peaks involved into the transitions.

To analyze the JSR spectra, reference PES of species in the literature were used along with calculated PES for several compounds of $m/z = 72, 84, 86$ and 88 reported for the first time and obtained via Franck-Condon simulations on the basis of high-level quantum chemistry calculations. These simulated PES have a critical role in the detection of products since the experimental literature is often very limited, especially for reactive intermediates, and will also enrich the data base of vibronic footprints, which will be of interest to the increasing number of groups using mass-selected PES for analytical purposes.

As demonstrated already in flame environments, the i^2 PEPICO technique supports isomer identification up to relatively heavy masses (50 - 100 amu) and is an efficient diagnostic tool for complex chemical gas-phase combustion analysis. Interestingly, an unexplained significant general trend seems to appear: the i^2 PEPICO mass spectrometry is more sensitive to ketones than gas chromatography. This could imply needed revision in the current models largely validated on these later data.

For large masses, the isomeric sensitivity could be enhanced if a more complete database were available for all the possible isomers that would include for instance high resolution TPES. For JSR experiments, this technique complements nicely gas chromatography for the separation of stable compounds with the same m/z . Its major advantage compared to GC is that it can also be applied to the detection short-lived species, such as hydroperoxides which play a major role in chemistry of the low-temperature oxidation of hydrocarbons. The analysis of diones and ketohydroperoxides detected at m/z 100 & 118 in this work along with the investigation of their fragmentation processes is planned in the near future. We show also that i^2 PEPICO data coupled to FC simulations and ab initio determination of the adiabatic ionization energies represent a powerful method which complements the GC data analysis for the heavy species.

Generally, the spreading use of the PEPICO technique should be consider as a powerful complementary diagnostic method aimed at improving the use of alternatives fossil fuels such as those derived from biogenic sources. In this prospect, further experiments should be focused on the reactions of oxygenated and N-bearing species found in biomass-derived nitrogenated-fuels in order to further improve reaction mechanisms developed for a new generation of cleaner and efficient fuels. Note that the GC analysis with highly-oxygenated and N-bearing species is often more challenging than with species obtained during the hydrocarbon oxidation (species containing C, H, and one or two oxygen atoms).

Acknowledgement

We are grateful to the whole SOLEIL staff for smoothly running the facility under project 20180021. We warmly thank J.-F. Gil for his technical help around the SAPHIRS experiment. J.B. thanks the ERC Starting Grant PRIMCHEM, grant agreement n°636829 for financial support. M.H. acknowledge the use of the computing center MésoLUM of the LUMAT research federation (FR LUMAT 2764).

Supplementary material

The Supplementary Material provides the results from the temperature dependence of the ion signal at m/z 58, the sensitivity analysis for the procedure fitting of m/z 86, the comparison between mole fractions in the literature and the observed signal branching ratio for isomers at m/z 86 and the comparison of the PES for the isomers at m/z 56 and 72 with the experimental TPES measured in this work. The simulated vibrationally resolved electronic spectra are also provided in the Supplementary Material.

References

- [1] K. Kohse-Höinghaus, Combustion Chemistry Diagnostics for Cleaner Processes, Chem. - A Eur. J. 22 (2016) 13390–13401. doi:10.1002/chem.201602676.
- [2] C.K. Westbrook, M. Mehl, W.J. Pitz, G. Kukkadapu, S. Wagnon, K. Zhang, Multi-fuel surrogate chemical kinetic mechanisms for real world applications, Phys. Chem. Chem. Phys. 20 (2018) 10588–10606. doi:10.1039/C7CP07901J.
- [3] P. Dagaut, S.M. Sarathy, M.J. Thomson, A chemical kinetic study of n-butanol oxidation at elevated pressure in a jet stirred reactor, Proc. Combust. Inst. 32 (2009) 229–237. doi:10.1016/J.PROCI.2008.05.005.
- [4] M.H. Hakka, P.-A. Glaude, O. Herbinet, F. Battin-Leclerc, Experimental study of the oxidation of large surrogates for diesel and biodiesel fuels, Combust. Flame. 156 (2009) 2129–2144. doi:10.1016/J.COMBUSTFLAME.2009.06.003.
- [5] N. Hansen, T.A. Cool, P.R. Westmoreland, K. Kohse-Höinghaus, Recent contributions of flame-sampling molecular-beam mass spectrometry to a fundamental understanding of combustion chemistry, Prog. Energy Combust. Sci. 35 (2009) 168–191. doi:10.1016/J.PECS.2008.10.001.
- [6] Y. Li, F. Qi, Recent Applications of Synchrotron VUV Photoionization Mass Spectrometry: Insight into Combustion Chemistry, Acc. Chem. Res. 43 (2010) 68–78. doi:10.1021/ar900130b.
- [7] H. Hashemi, J.M. Christensen, L.B. Harding, S.J. Klippenstein, P. Glarborg, High-pressure oxidation of propane, Proc. Combust. Inst. 37 (2019) 461–468. doi:10.1016/j.proci.2018.07.009.

- 769 [8] D.F. Davidson, Z. Hong, G.L. Pilla, A. Farooq, R.D. Cook, R.K. Hanson, Multi-species
770 time-history measurements during n-heptane oxidation behind reflected shock
771 waves. *Combustion and flame* (2010) 157(10), 1899-1905.
- 772 [9] S.S. Goldsborough, S. Hochgreb, G. Vanhove, M.S. Wooldridge, H.J. Curran, C.-J. Sung,
773 Advances in rapid compression machine studies of low- and intermediate-temperature
774 autoignition phenomena, *Prog. Energy Combust. Sci.* 63 (2017) 1–78.
775 doi:10.1016/j.pecs.2017.05.002.
- 776 [10] E. Ranzi, A. Frassoldati, A. Stagni, M. Pelucchi, A. Cuoci, T. Faravelli, Reduced kinetic
777 schemes of complex reaction systems: Fossil and biomass-derived transportation fuels,
778 *Int. J. Chem. Kinet.* 46 (2014) 512–542. doi:10.1002/kin.20867.
- 779 [11] S.M. Sarathy, P. Oßwald, N. Hansen, K. Kohse-Höinghaus, Alcohol combustion
780 chemistry, *Prog. Energy Combust. Sci.* 44 (2014) 40–102.
781 doi:10.1016/J.PECS.2014.04.003.
- 782 [12] B. Duboc, G. Ribert, P. Domingo, Description of kerosene/air combustion with Hybrid
783 Transported-Tabulated Chemistry. *Fuel* (2018) 233, 146-158.
- 784 [13] M. Djokic, H.-H. Carstensen, K.M. Van Geem, G.B. Marin, The thermal decomposition
785 of 2,5-dimethylfuran, *Proc. Combust. Inst.* 34 (2013) 251–258.
786 doi:10.1016/J.PROCI.2012.05.066.
- 787 [14] O. Herbinet, S. Bax, P.-A. Glaude, V. Carré, F. Battin-Leclerc, Mass spectra of cyclic
788 ethers formed in the low-temperature oxidation of a series of n-alkanes, *Fuel*. 90 (2011)
789 528–535. doi:10.1016/j.fuel.2010.09.047.
- 790 [15] N. Lamoureux, X. Mercier, C. Western, J.F. Pauwels, P. Desgroux, NCN quantitative
791 measurement in a laminar low pressure flame, *Proc. Combust. Inst.* 32 (2009) 937–944.
792 doi:10.1016/J.PROCI.2008.06.043.
- 793 [16] C.A. Taatjes, N. Hansen, A. McIlroy, J.A. Miller, J.P. Senosiain, S.J. Klippenstein, F. Qi,
794 L. Sheng, Y. Zhang, T.A. Cool, J. Wang, P.R. Westmoreland, M.E. Law, T. Kasper, K.
795 Kohse-Höinghaus, Enols are common intermediates in hydrocarbon oxidation., *Science*.
796 308 (2005) 1887–9. doi:10.1126/science.1112532.
- 797 [17] M.B. Sajid, E. Es-sebbar, T. Javed, C. Fittschen, A. Farooq, Measurement of the Rate of
798 Hydrogen Peroxide Thermal Decomposition in a Shock Tube Using Quantum Cascade
799 Laser Absorption Near 7.7 μm , *Int. J. Chem. Kinet.* 46 (2014) 275–284.
800 doi:10.1002/kin.20827.
- 801 [18] K. Kohse-Höinghaus, R.S. Barlow, M. Aldén, J. Wolfrum, Combustion at the focus: laser
802 diagnostics and control, *Proc. Combust. Inst.* 30 (2005) 89–123.
803 doi:10.1016/J.PROCI.2004.08.274.
- 804 [19] R.K. Hanson, Applications of quantitative laser sensors to kinetics, propulsion and
805 practical energy systems, *Proc. Combust. Inst.* 33 (2011) 1–40.
806 doi:10.1016/J.PROCI.2010.09.007.
- 807 [20] J.H. Northern, A.W.J. Thompson, M.L. Hamilton, P. Ewart, Multi-species detection using
808 multi-mode absorption spectroscopy (MUMAS), *Appl. Phys. B*. 111 (2013) 627–635.
809 doi:10.1007/s00340-013-5382-9.
- 810 [21] Z. Wang, O. Herbinet, N. Hansen, F. Battin-Leclerc, Exploring hydroperoxides in
811 combustion: History, recent advances and perspectives, *Prog. Energy Combust. Sci.* 73
812 (2019) 132–181. doi:10.1016/J.PECS.2019.02.003.
- 813 [22] O. Herbinet, F. Battin-Leclerc, S. Bax, H. Le Gall, P.-A. Glaude, R. Fournet, Z. Zhou, L.
814 Deng, H. Guo, M. Xie, F. Qi, Detailed product analysis during the low temperature

- oxidation of n-butane, *Phys. Chem. Chem. Phys.* 13 (2011) 296–308.
doi:10.1039/C0CP00539H.
- [23] F. Battin-Leclerc, O. Herbinet, P.-A. Glaude, R. Fournet, Z. Zhou, L. Deng, H. Guo, M. Xie, F. Qi, New experimental evidences about the formation and consumption of ketohydroperoxides, *Proc. Combust. Inst.* 33 (2011) 325–331.
doi:10.1016/j.proci.2010.05.001.
- [24] D.L. Osborn, P. Zou, H. Johnsen, C.C. Hayden, C.A. Taatjes, V.D. Knyazev, S.W. North, D.S. Peterka, M. Ahmed, S.R. Leone, The multiplexed chemical kinetic photoionization mass spectrometer: A new approach to isomer-resolved chemical kinetics, *Rev. Sci. Instrum.* 79 (2008) 104103. doi:10.1063/1.3000004.
- [25] C.A. Taatjes, N. Hansen, D.L. Osborn, K. Kohse-Höinghaus, T.A. Cool, P.R. Westmoreland, “Imaging” combustion chemistry via multiplexed synchrotron-photoionization mass spectrometry, *Phys. Chem. Chem. Phys.* 10 (2008) 20–34.
doi:10.1039/B713460F.
- [26] F. Qi, Combustion chemistry probed by synchrotron VUV photoionization mass spectrometry, *Proc. Combust. Inst.* 34 (2013) 33–63. doi:10.1016/j.proci.2012.09.002.
- [27] J. Eland, *Photoelectron spectroscopy: an introduction to ultraviolet photoelectron spectroscopy in the gas phase*, Elsevier (2013).
- [28] T. Baer, P.M. Guyon, An historical introduction to threshold photoionization. *High-Resolution Laser Photoionization and Photoelectron Studies*, John Wiley Sons Chichester (1995) 1–20.
- [29] A. Bodi, P. Hemberger, D.L. Osborn, B. Sztáray, Mass-Resolved Isomer-Selective Chemical Analysis with Imaging Photoelectron Photoion Coincidence Spectroscopy, *J. Phys. Chem. Lett.* 4 (2013) 2948–2952. doi:10.1021/jz401500c.
- [30] D.L. Osborn, C.C. Hayden, P. Hemberger, A. Bodi, K. Voronova, B. Sztáray, Breaking through the false coincidence barrier in electron–ion coincidence experiments, *J. Chem. Phys.* 145 (2016) 164202. doi:10.1063/1.4965428.
- [31] A. Bodi, M. Johnson, T. Gerber, Z. Gengeliczki, B. Sztáray, T. Baer, Imaging photoelectron photoion coincidence spectroscopy with velocity focusing electron optics, *Rev. Sci. Instrum.* 80 (2009) 034101. doi:10.1063/1.3082016.
- [32] G.A. Garcia, H. Soldi-Lose, L. Nahon, A versatile electron-ion coincidence spectrometer for photoelectron momentum imaging and threshold spectroscopy on mass selected ions using synchrotron radiation, *Rev. Sci. Instrum.* 80 (2009) 023102. doi:10.1063/1.3079331.
- [33] G.A. Garcia, B.K. Cunha de Miranda, M. Tia, S. Daly, L. Nahon, DELICIOUS III: A multipurpose double imaging particle coincidence spectrometer for gas phase vacuum ultraviolet photodynamics studies, *Rev. Sci. Instrum.* 84 (2013) 053112.
doi:10.1063/1.4807751.
- [34] T. Baer, R.P. Tuckett, Advances in threshold photoelectron spectroscopy (TPES) and threshold photoelectron photoion coincidence (TPEPICO), *Phys. Chem. Chem. Phys.* 19 (2017) 9698–9723. doi:10.1039/C7CP00144D.
- [35] D. Felsmann, K. Moshhammer, J. Krüger, A. Lackner, A. Brockhinke, T. Kasper, T. Bierkandt, E. Akyildiz, N. Hansen, A. Lucassen, P. Oßwald, M. Köhler, G.A. Garcia, L. Nahon, P. Hemberger, A. Bodi, T. Gerber, K. Kohse-Höinghaus, Electron ionization, photoionization and photoelectron/photoion coincidence spectroscopy in mass-spectrometric investigations of a low-pressure ethylene/oxygen flame, *Proc. Combust. Inst.* 35 (2015) 779–786. doi:10.1016/J.PROCI.2014.05.151.

- [36] J. Krüger, G.A. Garcia, D. Felsmann, K. Moshhammer, A. Lackner, A. Brockhinke, L. Nahon, K. Kohse-Höinghaus, Photoelectron–photoion coincidence spectroscopy for multiplexed detection of intermediate species in a flame, *Phys. Chem. Chem. Phys.* 16 (2014) 22791–22804. doi:10.1039/C4CP02857K.
- [37] P. Oßwald, P. Hemberger, T. Bierkandt, E. Akyildiz, M. Köhler, A. Bodi, T. Gerber, T. Kasper, *In situ* flame chemistry tracing by imaging photoelectron photoion coincidence spectroscopy, *Rev. Sci. Instrum.* 85 (2014) 025101. doi:10.1063/1.4861175.
- [38] D. Krüger, P. Oßwald, M. Köhler, P. Hemberger, T. Bierkandt, T. Kasper, The fate of the OH radical in molecular beam sampling experiments, *Proc. Combust. Inst.* 37 (2019) 1563–1570. doi:10.1016/J.PROCI.2018.05.041.
- [39] T. Bierkandt, P. Hemberger, P. Oßwald, D. Krüger, M. Köhler, T. Kasper, Flame structure of laminar premixed anisole flames investigated by photoionization mass spectrometry and photoelectron spectroscopy, *Proc. Combust. Inst.* 37 (2019) 1579–1587. doi:10.1016/J.PROCI.2018.07.037.
- [40] J. Pieper, S. Schmitt, C. Hemken, E. Davies, J. Wullenkord, A. Brockhinke, J. Krüger, G.A. Garcia, L. Nahon, A. Lucassen, W. Eisfeld, K. Kohse-Höinghaus, Isomer Identification in Flames with Double-Imaging Photoelectron/Photoion Coincidence Spectroscopy (ⁱPEPICO) using Measured and Calculated Reference Photoelectron Spectra, *Zeitschrift Für Phys. Chemie.* 232 (2018) 153–187. doi:10.1515/zpch-2017-1009.
- [41] D. Felsmann, A. Lucassen, J. Krüger, C. Hemken, L.-S. Tran, J. Pieper, G.A. Garcia, A. Brockhinke, L. Nahon, K. Kohse-Höinghaus, Progress in Fixed-Photon-Energy Time-Efficient Double Imaging Photoelectron/Photoion Coincidence Measurements in Quantitative Flame Analysis, *Zeitschrift Für Phys. Chemie.* 230 (2016). doi:10.1515/zpch-2016-0760.
- [42] A. Rodriguez, O. Herbinet, Z. Wang, F. Qi, C. Fittschen, P.R. Westmoreland, F. Battin-Leclerc, Measuring hydroperoxide chain-branching agents during n-pentane low-temperature oxidation, *Proc. Combust. Inst.* 36 (2017) 333–342. doi:10.1016/J.PROCI.2016.05.044.
- [43] J. Bugler, K.P. Somers, E.J. Silke, H.J. Curran, Revisiting the Kinetics and Thermodynamics of the Low-Temperature Oxidation Pathways of Alkanes: A Case Study of the Three Pentane Isomers, *J. Phys. Chem. A.* 119 (2015) 7510–7527. doi:10.1021/acs.jpca.5b00837.
- [44] J. Bugler, A. Rodriguez, O. Herbinet, F. Battin-Leclerc, C. Togbé, G. Dayma, P. Dagaut, H.J. Curran, An experimental and modelling study of n-pentane oxidation in two jet-stirred reactors: The importance of pressure-dependent kinetics and new reaction pathways, *Proc. Combust. Inst.* 36 (2017) 441–448. doi:10.1016/J.PROCI.2016.05.048.
- [45] L. Nahon, N. de Oliveira, G.A. Garcia, J.-F. Gil, B. Pilette, O. Marcouillé, B. Lagarde, F. Polack, IUCr, DESIRS: a state-of-the-art VUV beamline featuring high resolution and variable polarization for spectroscopy and dichroism at SOLEIL, *J. Synchrotron Radiat.* 19 (2012) 508–520. doi:10.1107/S0909049512010588.
- [46] X. Tang, G.A. Garcia, J.-F. Gil, L. Nahon, Vacuum upgrade and enhanced performances of the double imaging electron/ion coincidence end-station at the vacuum ultraviolet beamline DESIRS, *Rev. Sci. Instrum.* 86 (2015) 123108. doi:10.1063/1.4937624.
- [47] O. Herbinet, F. Battin-Leclerc, Progress in Understanding Low-Temperature Organic Compound Oxidation Using a Jet-Stirred Reactor, *Int. J. Chem. Kinet.* 46 (2014) 619–639. doi:10.1002/kin.20871.

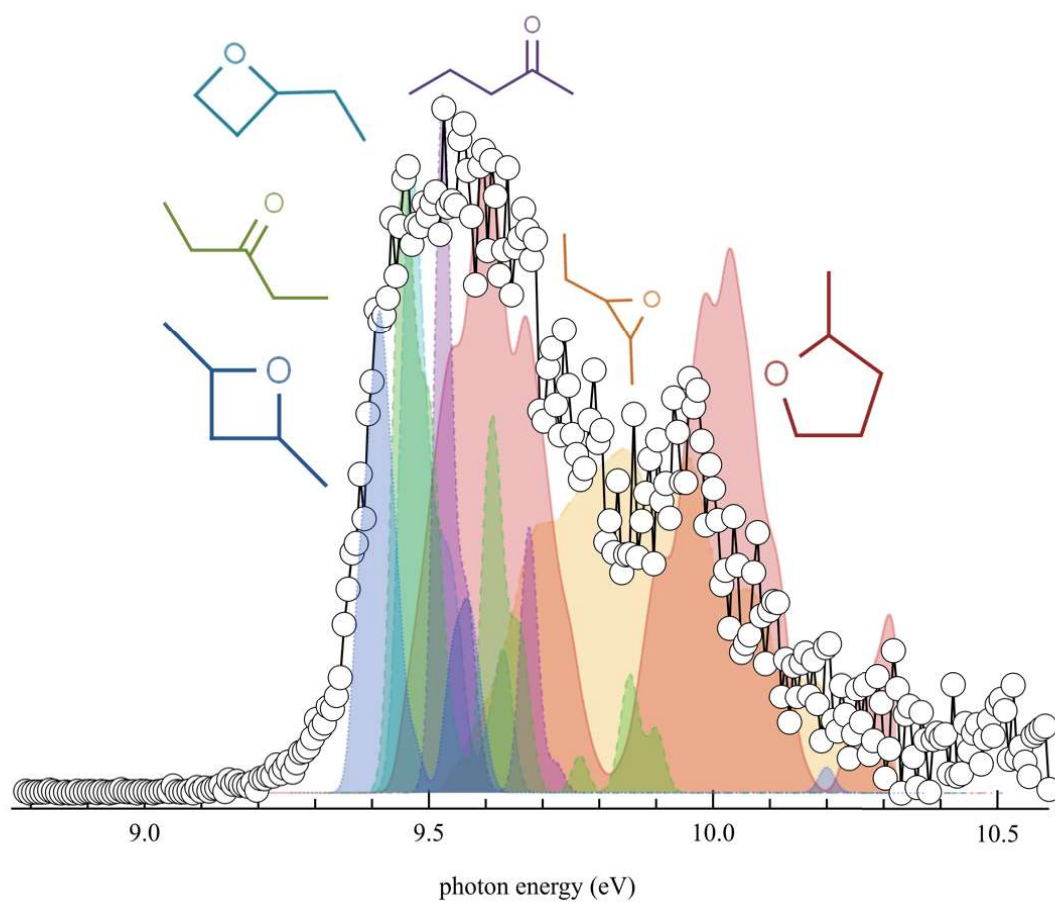
- [48] P. Azay, G.-M. Côme, Temperature Gradients in a Continuous Flow Stirred Tank Reactor, *Ind. Eng. Chem. Process Des. Dev.* 18 (1979) 754–756. doi:10.1021/i260072a030.
- [49] B. Mercier, M. Compin, C. Prevost, G. Bellec, R. Thissen, O. Dutuit, L. Nahon, Experimental and theoretical study of a differentially pumped absorption gas cell used as a low energy-pass filter in the vacuum ultraviolet photon energy range, *J. Vac. Sci. Technol. A Vacuum, Surfaces, Film.* 18 (2000) 2533. doi:10.1116/1.1288196.
- [50] K. Yoshino, Y. Tanaka, Absorption spectrum of krypton in the vacuum uv region, *J. Opt. Soc. Am.* 69 (1979) 159. doi:10.1364/JOSA.69.000159.
- [51] G.A. Garcia, L. Nahon, I. Powis, Two-dimensional charged particle image inversion using a polar basis function expansion, *Rev. Sci. Instrum.* 75 (2004) 4989–4996. doi:10.1063/1.1807578.
- [52] J.C. Pouilly, J.P. Schermann, N. Nieuwjaer, F. Lecomte, G. Grégoire, C. Desfrancois, G.A. Garcia, L. Nahon, D. Nandi, L. Poisson, M. Hochlaf, Photoionization of 2-pyridone and 2-hydroxypyridine, *Phys. Chem. Chem. Phys.* 12 (2010) 3566. doi:10.1039/b923630a.
- [53] M. Briant, L. Poisson, M. Hochlaf, P. de Pujo, M.-A. Gaveau, B. Soep, Ar₂ Photoelectron Spectroscopy Mediated by Autoionizing States, *Phys. Rev. Lett.* 109 (2012) 193401. doi:10.1103/PhysRevLett.109.193401.
- [54] J.A. Montgomery, M.J. Frisch, J.W. Ochterski, G.A. Petersson, A complete basis set model chemistry. VI. Use of density functional geometries and frequencies, *J. Chem. Phys.* 110 (1999) 2822–2827. doi:10.1063/1.477924.
- [55] Z. Chen, K.-C. Lau, G.A. Garcia, L. Nahon, D.K. Božanić, L. Poisson, M.M. Al-Mogren, M. Schwell, J.S. Francisco, A. Bellili, M. Hochlaf, Identifying Cytosine-Specific Isomers via High-Accuracy Single Photon Ionization, *J. Am. Chem. Soc.* 138 (2016) 16596–16599. doi:10.1021/jacs.6b10413.
- [56] C. Adamo, V. Barone, Toward reliable density functional methods without adjustable parameters: The PBE0 model, *J. Chem. Phys.* 110 (1999) 6158–6170. doi:10.1063/1.478522.
- [57] M. Frisch, G. Trucks, H. Schlegel, G. Scuseria, M. Robb, J. Cheeseman, G. Scalmani, V. Barone, B. Mennucci, G. Petersson, H. Nakatsuji, X. Li, M. Caricato, A. Marenich, J. Bloino, B.G. Janesko, R. Gomperts, B. Mennucci, H.P. Hratchian, J. V. Ortiz, A.F. Izmaylov, J.L. Sonnenberg, D. Williams-Young, F. Ding, F. Lipparini, F. Egidi, J. Goings, B. Peng, A. Petrone, T. Henderson, D. Ranasinghe, V.G. Zakrzewski, J. Gao, N. Rega, G. Zheng, W. Liang, M. Hada, M. Ehara, K. Toyota, R. Fukuda, J. Hasegawa, M. Ishida, T. Nakajima, Y. Honda, O. Kitao, H. Nakai, T. Vreven, K. Throssell, J.A. Montgomery Jr., J.E. Peralta, F. Ogliaro, M. Bearpark, J.J. Heyd, E. Brothers, K.N. Kudin, V.N. Staroverov, T. Keith, R. Kobayashi, J. Normand, K. Raghavachari, A. Rendell, J.C. Burant, S.S. Iyengar, J. Tomasi, M. Cossi, J.M. Millam, M. Klene, C. Adamo, R. Cammi, J.W. Ochterski, R.L. Martin, K. Morokuma, O. Farkas, J.B. Foresman, D.J. Fox, Gaussian 09, Revision A.02, Gaussian, Inc., Wallingford CT. 200 (2009) 28.
- [58] T.H. Dunning, Gaussian basis sets for use in correlated molecular calculations. I. The atoms boron through neon and hydrogen, *J. Chem. Phys.* 90 (1989) 1007–1023. doi:10.1063/1.456153.
- [59] R.A. Kendall, T.H. Dunning, R.J. Harrison, Electron affinities of the first-row atoms revisited. Systematic basis sets and wave functions, *J. Chem. Phys.* 96 (1992) 6796–6806. doi:10.1063/1.462569.
- [60] J. Bloino, M. Biczysko, F. Santoro, V. Barone, General Approach to Compute

- Vibrationally Resolved One-Photon Electronic Spectra, *J. Chem. Theory Comput.* 6 (2010) 1256–1274. doi:10.1021/ct9006772.
- [61] V. Barone, J. Bloino, M. Biczysko, F. Santoro, Fully Integrated Approach to Compute Vibrationally Resolved Optical Spectra: From Small Molecules to Macrosystems, *J. Chem. Theory Comput.* 5 (2009) 540–554. doi:10.1021/ct8004744.
- [62] J. Bloino, M. Biczysko, O. Crescenzi, V. Barone, Integrated computational approach to vibrationally resolved electronic spectra: Anisole as a test case, *J. Chem. Phys.* 128 (2008) 244105. doi:10.1063/1.2943140.
- [63] J. Bloino, A. Baiardi, M. Biczysko, Aiming at an accurate prediction of vibrational and electronic spectra for medium-to-large molecules: An overview, *Int. J. Quantum Chem.* 116 (2016) 1543–1574. doi:10.1002/qua.25188.
- [64] T.B. Adler, H.-J. Werner, Local explicitly correlated coupled-cluster methods: Efficient removal of the basis set incompleteness and domain errors, *J. Chem. Phys.* 130 (2009) 241101. doi:10.1063/1.3160675.
- [65] T.B. Adler, G. Knizia, H.-J. Werner, A simple and efficient CCSD(T)-F12 approximation, *J. Chem. Phys.* 127 (2007) 221106. doi:10.1063/1.2817618.
- [66] G. Knizia, T.B. Adler, H.-J. Werner, Simplified CCSD(T)-F12 methods: Theory and benchmarks, *J. Chem. Phys.* 130 (2009) 054104. doi:10.1063/1.3054300.
- [67] T.B. Adler, H.-J. Werner, F.R. Manby, Local explicitly correlated second-order perturbation theory for the accurate treatment of large molecules, *J. Chem. Phys.* 130 (2009) 054106. doi:10.1063/1.3040174.
- [68] K.E. Yousaf, K.A. Peterson, Optimized auxiliary basis sets for explicitly correlated methods, *J. Chem. Phys.* 129 (2008) 184108. doi:10.1063/1.3009271.
- [69] H.-J. Werner, P.J. Knowles, G. Knizia, F.R. Manby, M. Schütz, Molpro: a general-purpose quantum chemistry program package, *Wiley Interdiscip. Rev. Comput. Mol. Sci.* 2 (2012) 242–253. doi:10.1002/wcms.82.
- [70] Y. Pan, K.-C. Lau, L. Poisson, G.A. Garcia, L. Nahon, M. Hochlaf, Slow Photoelectron Spectroscopy of 3-Hydroxyisoquinoline, *J. Phys. Chem. A.* 117 (2013) 8095–8102. doi:10.1021/jp311615u.
- [71] Y. Pan, K.-C. Lau, M.M. Al-Mogren, A. Mahjoub, M. Hochlaf, Theoretical studies of 2-quinolinol: Geometries, vibrational frequencies, isomerization, tautomerism, and excited states, *Chem. Phys. Lett.* 613 (2014) 29–33. doi:10.1016/J.CPLETT.2014.08.033.
- [72] M. Hochlaf, Advances in spectroscopy and dynamics of small and medium sized molecules and clusters, *Phys. Chem. Chem. Phys.* 19 (2017) 21236–21261. doi:10.1039/C7CP01980G.
- [73] Y. Majdi, M. Hochlaf, Y. Pan, K.-C. Lau, L. Poisson, G.A. Garcia, L. Nahon, M.M. Al-Mogren, M. Schwell, Theoretical and Experimental Photoelectron Spectroscopy Characterization of the Ground State of Thymine Cation, *J. Phys. Chem. A.* 119 (2015) 5951–5958. doi:10.1021/jp510716c.
- [74] H.Y. Zhao, K.-C. Lau, G.A. Garcia, L. Nahon, S. Carniato, L. Poisson, M. Schwell, M.M. Al-Mogren, M. Hochlaf, Unveiling the complex vibronic structure of the canonical adenine cation, *Phys. Chem. Chem. Phys.* 20 (2018) 20756–20765. doi:10.1039/C8CP02930J.
- [75] M. Bobeldijk, W.J. Van der Zande, P.G. Kistemaker, Simple models for the calculation of photoionization and electron impact ionization cross sections of polyatomic molecules, *Chemical physics*, 179(2) (1994) 125-130. doi:10.1016/0301-0104(93)E0376-7

- [76] B. Niu, Y. Bai, D.A. Shirley, High resolution He I α photoelectron spectroscopy of H₂CCO and D₂CCO using supersonic molecular beams, *Chem. Phys. Lett.* 201 (1993) 217–222. doi:10.1016/0009-2614(93)85059-W.
- [77] G. Bieri, F. Burger, E. Heilbronner, J.P. Maier, Valence Ionization Energies of Hydrocarbons, *Helv. Chim. Acta.* 60 (1977) 2213–2233. doi:10.1002/hlca.19770600714.
- [78] B. Yang, J. Wang, T.A. Cool, N. Hansen, S. Skeen, D.L. Osborn, Absolute photoionization cross-sections of some combustion intermediates, *Int. J. Mass Spectrom.* 309 (2012) 118–128. doi:10.1016/j.ijms.2011.09.006.
- [79] J.C. Person, P.P. Nicole, Isotope Effects in the Photoionization Yields and the Absorption Cross Sections for Acetylene, Propyne, and Propene, *J. Chem. Phys.* 53 (1970) 1767–1774. doi:10.1063/1.1674254.
- [80] D. Chadwick, A. Katrib, Photoelectron spectra of acetaldehyde and acetyl halides, *J. Electron Spectros. Relat. Phenomena.* 3 (1974) 39–52. doi:10.1016/0368-2048(74)80073-3.
- [81] K. Johnson, I. Powis, C.J. Danby, A photoelectron—photoion coincidence study of acetaldehyde and ethylene oxide molecular ions, *Chem. Phys.* 70 (1982) 329–343. doi:10.1016/0301-0104(82)88103-2.
- [82] W.R. Stevens, A. Bodi, T. Baer, Dissociation Dynamics of Energy Selected, Propane, and *i*-C₃H₇X⁺ Ions by iPEPICO: Accurate Heats of Formation of *i*-C₃H₇⁺, *i*-C₃H₇Cl, *i*-C₃H₇Br, and *i*-C₃H₇I, *J. Phys. Chem. A.* 114 (2010) 11285–11291. doi:10.1021/jp104200h.
- [83] D.J. Knowles, A.J.C. Nicholson, Ionization energies of formic and acetic acid monomers, *J. Chem. Phys.* 60 (1974) 1180–1181. doi:10.1063/1.1681132.
- [84] A.J. Yench, M.R.F. Siggel-King, G.C. King, A.E.R. Malins, M. Eypper, Threshold photoelectron spectroscopy of acetaldehyde and acrolein, *J. Electron Spectros. Relat. Phenomena.* 187 (2013) 65–71. doi:10.1016/J.ELSPEL.2013.04.005.
- [85] H. Bock, T. Hirabayashi, S. Mohmand, Gasphasen-Reaktionen, 21. Thermische Erzeugung von Alkyl- und Halogenketenen, *Chem. Ber.* 114 (1981) 2595–2608. doi:10.1002/cber.19811140722.
- [86] E. Ranzi, C. Cavallotti, A. Cuoci, A. Frassoldati, M. Pelucchi, T. Faravelli, New reaction classes in the kinetic modeling of low temperature oxidation of n-alkanes, *Combust. Flame.* 162 (2015) 1679–1691. doi:10.1016/J.COMBUSTFLAME.2014.11.030.
- [87] A.A. Bredikhin, Photoelectron spectra of alkoxyacetylenes: σ , α -interactions with simultaneous participation of both oxygen unshared pairs, *Bull. Acad. Sci. USSR Div. Chem. Sci.* 40 (1991) 1583–1587. doi:10.1007/BF01172255.
- [88] C.E. van Der Meij, J. Van Eck, A. Niehaus, The decomposition of C₄H₈⁺ complexes at controlled internal energies, *Chem. Phys.* 130 (1989) 325–334. doi:10.1016/0301-0104(89)87061-2.
- [89] J. Dannacher, J.-P. Stadelmann, Behavior of excited C₃H₆O⁺ cations: a He-I α photoelectron-photoion coincidence study of propanal, *Int. J. Mass Spectrom.* 208 (2001) 147–157. doi:10.1016/S1387-3806(01)00387-6.
- [90] Emma E. Rennie, Anne-Marie Boulanger, P.M. Mayer, D.M. Holland, D.A. Shaw, L. Cooper, L.G. Shpinkova, A Photoelectron and TPEPICO Investigation of the Acetone Radical Cation, (2006). doi:10.1021/JP0616866.
- [91] Z. Zhou, M. Xie, Z. Wang, F. Qi, Determination of absolute photoionization cross-sections of aromatics and aromatic derivatives, *Rapid Commun. Mass Spectrom.* 23 (2009) 3994–4002. doi:10.1002/rcm.4339.

- [92] K. Watanabe, T. Nakayama, J. Mottl, Ionization potentials of some molecules, *J. Quant. Spectrosc. Radiat. Transf.* 2 (1962) 369–382. doi:10.1016/0022-4073(62)90023-7.
- [93] J. Wang, B. Yang, T.A. Cool, N. Hansen, T. Kasper, Near-threshold absolute photoionization cross-sections of some reaction intermediates in combustion, *Int. J. Mass Spectrom.* 269 (2008) 210–220. doi:10.1016/J.IJMS.2007.10.013.
- [94] T.A. Cool, J. Wang, K. Nakajima, C.A. Taatjes, A. McIlroy, Photoionization cross sections for reaction intermediates in hydrocarbon combustion, *Int. J. Mass Spectrom.* 247 (2005) 18–27. doi:10.1016/J.IJMS.2005.08.018.
- [95] W. von Niessen, G. Bieri, L. Åsbrink, 30.4-nm He (II) photoelectron spectra of organic molecules: Part III. Oxo-compounds (C, H, O), *J. Electron Spectros. Relat. Phenomena.* 21 (1980) 175–191. doi:10.1016/0368-2048(80)85046-8.
- [96] A. Jalan, I.M. Alecu, R. Meana-Pañeda, J. Aguilera-Iparraguirre, K.R. Yang, S.S. Merchant, D.G. Truhlar, W.H. Green, New Pathways for Formation of Acids and Carbonyl Products in Low-Temperature Oxidation: The Korcek Decomposition of γ -Ketohydroperoxides, *J. Am. Chem. Soc.* 135 (2013) 11100–11114. doi:10.1021/ja4034439.
- [97] J.-P. Morizur, J. Mercier, M. Sarraf, 2-substituted-2,3-dihydro-4H-pyran: Competition between ‘retro Diels-Alder’ fragmentation and substituent loss, *Org. Mass Spectrom.* 17 (1982) 327–330. doi:10.1002/oms.1210170708.
- [98] W.-C. Tam, D. Yee, C.E. Brion, Photoelectron spectra of some aldehydes and ketones, *J. Electron Spectros. Relat. Phenomena.* 4 (1974) 77–80. doi:10.1016/0368-2048(74)80045-9.
- [99] K. Seki, H. Inokuchi, The Ultraviolet Photoelectron Spectroscopy of Aliphatic Hydrocarbons and Tetramethylsilane in the Solid State, *Bull. Chem. Soc. Jpn.* 56 (1983) 2212–2219. doi:10.1246/bcsj.56.2212.
- [100] F. Buda, R. Bounaceur, V. Warth, P.A. Glaude, R. Fournet, F. Battin-Leclerc, Progress toward a unified detailed kinetic model for the autoignition of alkanes from C₄ to C₁₀ between 600 and 1200 K, *Combust. Flame.* 142 (2005) 170–186. doi:10.1016/J.COMBUSTFLAME.2005.03.005.

Graphical Abstract



1087